

Review

# Deep Eutectic Solvent-Mediated Electrocatalysts for Water Splitting

Chenyun Zhang <sup>1</sup>, Yongqi Fu <sup>1</sup>, Wei Gao <sup>2</sup>, Te Bai <sup>1</sup>, Tianyi Cao <sup>1</sup>, Jianjiao Jin <sup>1</sup> and Bingwei Xin <sup>2,\*</sup><sup>1</sup> School of Intelligent Manufacturing, Wuxi Vocational College of Science and Technology, Wuxi 214028, China<sup>2</sup> College of Chemistry and Chemical Engineering, Dezhou University, Dezhou 253023, China

\* Correspondence: xinbingwei@dzu.edu.cn; Tel.: +86-13685345517

**Abstract:** As green, safe, and cheap solvents, deep eutectic solvents (DESs) provide tremendous opportunities to open up attractive perspectives for electrocatalysis. In this review, the achievement of DESs in the preparation of catalysts for electrolytic water splitting is described in detail according to their roles combined with our own work. DESs are generally employed as green media, templates, and electrolytes. A large number of hydrogen bonds in DESs result in supramolecular structures which have the ability to shape the morphologies of nanomaterials and then tune their performance. DESs can also serve as reactive reagents of metal electrocatalysts through directly participating in synthesis. Compared with conventional heteroatom sources, they have the advantages of high safety and designability. The “all-in-one” transformation strategy is expected to realize 100% atomic transformation of reactants. The aim of this review is to offer readers a deeper understanding on preparing DES-mediated electrocatalysts with higher performance for water splitting.

**Keywords:** deep eutectic solvent; metal catalyst; electrocatalysis; water splitting



**Citation:** Zhang, C.; Fu, Y.; Gao, W.; Bai, T.; Cao, T.; Jin, J.; Xin, B. Deep Eutectic Solvent-Mediated Electrocatalysts for Water Splitting. *Molecules* **2022**, *27*, 8098. <https://doi.org/10.3390/molecules27228098>

Academic Editor: Joaquín García Álvarez

Received: 21 October 2022

Accepted: 16 November 2022

Published: 21 November 2022

**Publisher's Note:** MDPI stays neutral with regard to jurisdictional claims in published maps and institutional affiliations.



**Copyright:** © 2022 by the authors. Licensee MDPI, Basel, Switzerland. This article is an open access article distributed under the terms and conditions of the Creative Commons Attribution (CC BY) license (<https://creativecommons.org/licenses/by/4.0/>).

## 1. Introduction

Facing the serious challenges of energy crisis and environmental pollution, increasing attention is being focused on green energy, such as biodiesel, solar, wind, etc. [1,2]. H<sub>2</sub> is becoming one of the most promising prospective green energy sources due to its high efficiency, zero emissions and renewability [3,4]. Electrocatalytic water splitting is a significant technological method of producing hydrogen. This reaction involves two half reactions: hydrogen evolution reaction (HER) and oxygen evolution reaction (OER) [5–8]. For this reaction, one of the most critical issues is exploring efficient electrocatalysts. In the process of preparing catalysts, obtaining high efficiency catalysts and simultaneously reducing environmental pollution is a core issue of research. Therefore, the application of green solvents and the realization of high atomic conversion of the reactants has always been the goal of people's pursuit. In recent decades, ionic liquids (ILs) have been extensively studied [9–11]. ILs are composed of large organic cations and small organic or inorganic anions, thereby being liquid below 100 °C. Their special liquid structures and properties have made great achievements possible in catalytic chemistry. Nevertheless, the “greenness” of ILs is becoming challenged because their biodegradability, biocompatibility and sustainability are poor [12–14]. In addition, ILs are rather complex to purify, and expensive, resulting in certain restrictions in industrial production.

Under this background, deep eutectic solvents (DESs), a kind of alternative to ILs, have begun to draw people's attention [15–17]. In 2003, Abbott and co-workers combined the choline chloride (ChCl, HOC<sub>2</sub>H<sub>4</sub>N<sup>+</sup>(CH<sub>3</sub>)<sub>3</sub>Cl<sup>−</sup>) (melting point, T<sub>m</sub> ≈ 302 °C) and urea (T<sub>m</sub> ≈ 133 °C) with a mole fraction of 1:2 and found that they finally presented as liquid with T<sub>m</sub> ≈ 12 °C. They put forward the concept of “deep eutectic solvents” for the first time, opening up a new era in the application of eutectic solvents [18]. DESs refer to a two- or three-component combination of a hydrogen bond acceptor (HBA) and hydrogen bond donor (HBD) in a certain molar ratio [19–23]. The strong hydrogen bonds between HBA and HBD drive the mixture to liquid, and the freezing point of DESs is

much lower than that of any component. HBAs are usually quaternary ammoniums (e.g., ChCl, tetra propyl ammonium bromide (TPAB),  $N_{8881}Cl$ , etc.), phosphonium salts (e.g.,  $P_{14666}Cl$ ,  $P_{4444}Cl$ , etc.), hydrated metal salts (e.g.,  $NiCl_2 \cdot 6H_2O$ ,  $CoCl_2 \cdot 6H_2O$ , etc.), or Lewis acid metal salts (e.g.,  $FeCl_3$ ,  $ZnCl_2$ , etc.) [24–28]. Quaternary ammonium salts ( $R^1R^2R^3R^4N^+ \cdot X^-$ ), especially ChCl, are the most common HBAs. HBDs are generally amides, carboxylic acids, polyols, and so on. DESs can be divided into five types [24], as shown in Table 1. Type I refers to the combination of quaternary ammonium salts and metal chlorides. Type II DESs are composed of quaternary ammonium salts and metal chloride hydrates, such as ChCl/ $NiCl_2 \cdot 6H_2O$  and so on. Type III consists of quaternary ammonium salts and HBDs (usually organic molecular components, such as amide, carboxylic acid, or polyol, etc.). ChCl/urea, ChCl/ethylene glycol (EG) as well as ChCl/glycerol are popular DESs. Type IVs are made of metal chloride hydrates and HBDs [25]. These four DESs occupy a dominant position, in which most of the studies have focused on Type III. At least one of HBA and HBD is an ionic species, which mainly interacts with strong hydrogen bonds, making the resulting mixture hydrophilic. However, a relatively new category of Type V DESs have been found, which consist of nonionic molecular HBAs and HBDs [26]. Although these compounds lack ionic contribution, a large number of hydrogen bonds make them retain the characteristics of DESs' melting point. The clever design of HBAs and HBDs makes DESs “designer solvents”. The large number of hydrogen bonds between HBAs and HBDs induce DESs to possess special properties, just as for ILs. In addition, DESs behave with high ionic charge, dielectric constant and polarity, ideal conductivity and wide electrochemical potential window, nonvolatility, good thermal stability, etc. [27,28]. Therefore, DESs are considered as IL analogues [29]. Compared with ILs, DESs have advantages over ILs. They are low-cost, nontoxic, and biodegradable (Figure 1). In particular, they are easier to prepare. DESs have many preparation methods. The most common method includes heating and stirring the components of HBAs and HBDs until they form a uniform liquid. Other methods of preparing DESs involve vacuum evaporation, grinding and freeze drying. These preparation methods rarely require solvents, while sometimes requiring minimum water content. Therefore, there is no purification step, which is one of the biggest advantages over ILs. The economical and efficient preparation methods are more promising in industry. Since they have been discovered, DESs are recognized as cheap, renewable and green solvents. They have been rapidly applied in chemistry, biology, physics, engineering, and many other fields [30]. In the field of functional materials, DESs have attracted great attention. In 2004, Morris and his team carried out the preparation of inorganic materials in DESs and raised the concept of “ionothermal synthesis” [20]. This synthesis technology not only makes full use of the special modulation of DESs to inorganic micro/nanomaterials, but also avoids the danger of hydrothermal pressure because of the high stability and ignorable vapor pressure of DESs. Moreover, the favorable conductivity and wide potential window of DESs make them widely used as electrolytes to prepare inorganic nanomaterials by electrodeposition technology. DESs can be used as green media, templates, and sacrificial reagents in the preparation of micro/nanomaterials (Figure 1) [31,32]. Although the research on DESs is in infancy compared with ILs, the preparation of electrocatalysts assisted by DESs has become a new trend [33–36].

Compared with other solvents, DESs as media and sacrificial reagents can express the advantages in materials chemistry and catalytic chemistry in the following ways:

- (1) DESs are considered emerging green solvents and promisingly soft templates [37]. This is because DESs have special properties. Firstly, they exhibit fine solubility for metal salts, so that they are beneficial in synthesizing catalysts. Secondly, the low vapor pressure and high thermal stability of DESs allow the progress of reactions at high temperature and ambient pressure, avoiding the danger of high pressure. Thirdly, owing to the hydrogen bond, highly ionic strength and the viscosity of DESs, the microenvironment is different from that in conventional solvents. The supramolecular nature of DESs can tune structures and sizes of micro/nanomaterials.

- (2) DESs can serve as active reactants to prepare catalysts. Their designability makes them P, S, N, C or metals sources (such as Fe, Co, Ni and so on) to form phosphides, sulfides, nitrides, carbides or metal-based catalysts [38,39]. Compared with traditional heteroatom sources, they are safe and green. Moreover, owing to the influence of the special liquid structure of DESs during the reaction process, the obtained products show different structures and performance from those obtained from the conventional reactants. In addition, the conversion of DESs into electrocatalysts can reduce waste emissions and simplify operation processes.
- (3) The unique physicochemical characteristics of DESs result in different nucleation and growth mechanisms from those in conventional solvents through charge neutralization, changes in reduction potential as well as chemical activity, and determination of growth along the preferred crystallographic directions. In addition, DESs are able to change the activity order of metals, leading to some displacement reactions that cannot occur in aqueous solutions being undertaken in DESs [40].

**Table 1.** Classification of DESs.

Type	Composition	Terms	Example	Ref.
Type I	$R^1R^2R^3R^4N^+ \cdot X^- + MCl_x$	X is a Lewis base, generally a halide anion; M = Zn, Sn, Fe, Al, Ga, In, etc.	ChCl/ZnCl <sub>2</sub>	[24]
Type II	$R^1R^2R^3R^4N^+ \cdot X^- + MCl_x \cdot yH_2O$	X is a Lewis base, generally a halide anion; M = Cr, Co, Cu, Ni, Fe, etc	ChCl/NiCl <sub>2</sub> ·6H <sub>2</sub> O	[24]
Type III	$R^1R^2R^3R^4N^+ \cdot X^- + HBD$	HBDs include RCONH <sub>2</sub> , RCOOH, ROH, etc	ChCl/urea, ChCl/EG, ChCl/glycerol	[25]
Type IV	$MCl_x \cdot yH_2O + HBD$	M = Zn, Sn, Fe, Al, etc; HBDs include RCONH <sub>2</sub> , RCOOH, ROH, etc		[25]
Type V	nonionic, molecular HBAs +HBDs		thymol/menthol thymol/lidocaine	[26]

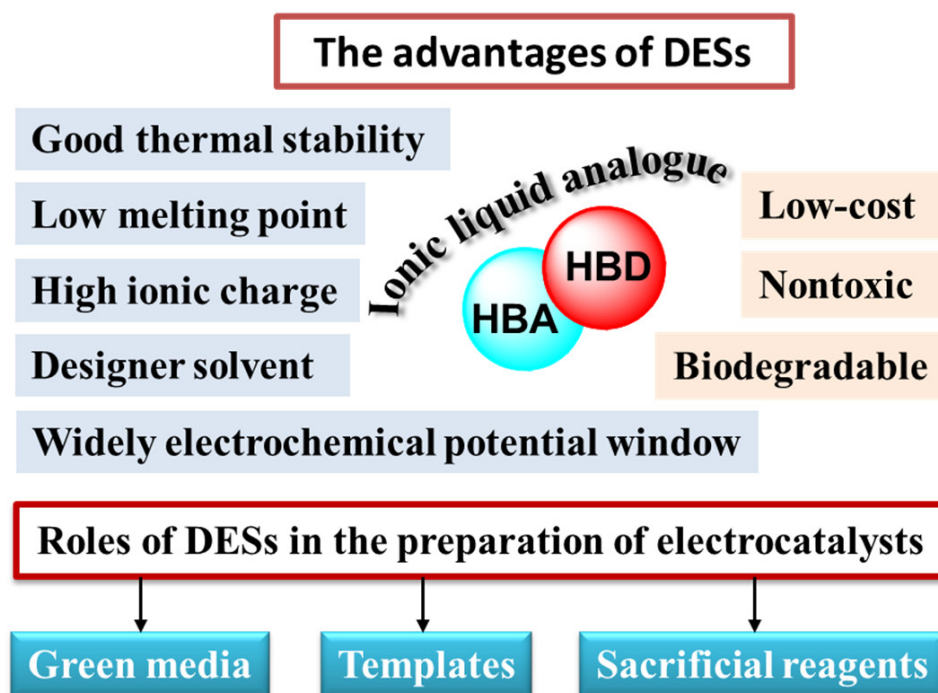


**Figure 1.** The advantages and roles of DESs in the preparation of electrocatalysts.

To date, DESs have been widely explored in the preparation of catalysts for the electrolysis of water. Therefore, the progress in DES-mediated electrocatalysts for HER and OER is overviewed in detail in this review. This article is divided into four sections. Section 1 is the Introduction section, describing DESs and their advantages in the preparation of electrochemical catalysts. In Section 2, we describe DESs as both solvent and structure-directed reagents simultaneously for the synthesis of electrocatalysts. Section 3 discusses that DESs themselves are employed as reactive reagents to synthesize catalysts as sources of N, S, P, C, etc., while (hydrated) metal chloride-based DESs can provide a series of metallic elements, such as Fe, Co, Ni and Mn, etc. In Section 4, we draw conclusions from this review, while analyzing issues as well as prospects for further study on the evolution of DES-mediated electrocatalysts.

With the comprehensive development of DESs in various fields, a series of excellent reviews on DESs have been published focusing on food analysis, extraction, dissolution, organic synthesis, etc. [41–43]. Reviews with unique insights are also reported in the field of synthesis of functional materials [44,45]. However, up until now, no review has focused on the preparation of water splitting catalysts mediated by DESs. In this review, we made a detailed summary of this direction. We highlighted the advantages of DESs in the synthesis of inorganic electrocatalysts by comparing with traditional preparation methods. Meanwhile, our group is concerned with the 100% utilization of DESs and proposed an “all-in-one” DES strategy, which reduces emissions and minimizes pollution. We hope that readers will be able to follow the development trend in this field by reading this review, so that novel DESs may be designed and catalysts with novel structures and excellent properties may be prepared. Given the rapid development of this issue, the progress presented here covers about the period from January 2010 to October 2022.

## 2. Deep Eutectic Solvents as Both Green Solvents and Structure-Directed Reagents Simultaneously for the Preparation of HER and OER Electrocatalysts

With the rapid development of the concept of green environmental protection, DESs are one of the most investigated new green solvents [46,47]. Compared with traditional solvents, the low vapor pressure and high thermal stability of DESs allow the progress of reactions at high temperature and ambient pressure, avoiding the danger of high pressure. Although DESs are recognized as an alternative to ILs, DESs have advantages over ILs, such as low cost, natural origin, lower toxicity, and better environmental compatibility. Studies have shown that DESs are generally less cytotoxic than imidazolyl and pyridyl ILs, and can maintain high activity and unexpected stability of enzymes [48,49]. The safety of DESs makes them widely used in liquid-liquid, liquid-solid, and combined extractions [50]. In terms of the preparation of ILs and DESs, the synthesis of ILs usually needs a long time, which involves multiple synthetic steps with various reagents and organic volatile solvents. In addition, by-products and wastes are generated during the preparation of ILs. However, DESs can be simply prepared by a heating or grinding method with 100% yield. DESs are relatively simple and inexpensive to produce, and do not pose any major postpurification or disposal problems [51]. DESs also are promisingly soft templates. Owing to the hydrogen bond, highly ionic strength, and viscosity of DESs, the microenvironment is different from that in conventional solvents. The supramolecular nature of DESs can tune the structures and size of micro/nanomaterials. DESs are widely used in the preparation of electrocatalysts (Table 2).

Nickel-based materials have been promising electrocatalysts for HER and OER (Figure 2). Their preparation in DESs has been extensively researched in recent years. Studies have found that DESs as electrolytes are better than aqueous electrolytes due to their high ionic conductivity and wide electrochemical window [52–54]. Comparing aqueous electrolytes with DESs, many factors, including viscosity, conductivity and ionic property, are different. In DESs,  $\text{NiCl}_2 \cdot 6\text{H}_2\text{O}$  displayed significant stable behavior due to coordination between DESs and  $\text{Ni}^{2+}$ . In aqueous and DES, Ni disposition can be obtained with similar disposition rates affected by many factors. However, the Ni disposition obtained from  $\text{ChCl}/\text{EG}$  is

considerably harder than that obtained from aqueous solutions, while presenting a different morphology. Ni nanoparticles obtained in DES via electrodeposition possessed smaller sizes and more uniform morphology than those obtained from an acetate buffer under similar conditions [55]. Therefore, Ni nanoparticles prepared by DES have high catalytic performance. Meanwhile, DES electrolytes are inexpensive, non-corrosive, compatible with electrode assemblies, and environmentally friendly, making them sustainable and cost-effective [56].

Further studies find that the compositions of DESs also affect the structure of the catalysts during the electrodeposition process. ChCl/urea and ChCl/EG DESs produced Ni films with different properties due to their different growth processes and assembling behaviors (Figure 2a). ChCl/EG has lower viscosity and higher conductivity than ChCl/urea. The diffusion coefficient of  $\text{Ni}^{2+}$  species in ChCl/urea is much slower than that in ChCl/EG. In addition, their coordination environment is also different. Therefore, the Ni films obtained from ChCl/EG possess different nanoparticles from those produced in ChCl/urea [57,58].

Different nickel salts behave differently in DESs, resulting in different nickel-based catalysts. For instance, replacing pure  $\text{NiCl}_2$  with the mixture of  $\text{NiCl}_2$  and  $\text{Ni}(\text{NO}_3)_2$  led to obtaining Ni/Ni(OH)<sub>2</sub> films on the substrate in ChCl/EG electrolyte via electrodeposition [59]. The reason should be that the reduction of  $\text{NO}_3^-$  at a reducing potential generated  $\text{OH}^-$ . Therefore, Ni(OH)<sub>2</sub> was formed on the surface of Ni films. Clearly, the presence of  $\text{NO}_3^-$  played a crucial role in the component of the product in the deposition process. The as-obtained Ni/Ni(OH)<sub>2</sub> electrode required overpotentials of 110 mV for HER as well as 320 mV for OER to deliver a current density of  $10 \text{ mA cm}^{-2}$ .

Although nickel itself is a promising Pt alternative metal for catalyzing HER, the strong adsorption capacity for hydrogen causes the desorption of  $\text{H}_2$  to be relatively slow. Doped S or P on Ni can tailor its electronic structure to optimize the intrinsic activity as well as the adsorption free energy of  $\text{H}_2$ . Therefore, metal sulfides as electrocatalysts for  $\text{H}_2\text{O}$  splitting have always been a research hotspot. Zhang et al. used an electrodeposition method to synthesize S-doped Ni microspherated films directly grown on Cu wire in ChCl/EG electrolyte [60]. They found that doping of S led to high amounts of oxygen vacancy on the surface. The influence of the ratio of Ni to S on the morphology and performance of the catalyst was investigated.  $\text{NiS}_{0.25}$  nanospheres possessed the biggest surface area among a series of catalysts with different Ni/S ratios. The synergistic effect of morphology and oxygen vacancies led  $\text{NiS}_{0.13}$  nanospheres to hold the highest electrocatalytic activity for HER. It showed a small overpotential of 54 mV to reach  $10 \text{ mA cm}^{-2}$  and continuous stability of 60 h in 1.0 M KOH solution.

More strikingly, DESs can alter the redox potential of metals, causing metal activity sequences different from those in aqueous solutions [61]. It is well known that the displacement reaction between Cu and  $\text{Ni}^{2+}$  is impossible without a chemical reducing agent in aqueous solution. However, experiments show that the redox potential of  $\text{Ni}^{2+}/\text{Ni}$  in ChCl/EG is  $-0.154 \text{ V}$ , while that of  $\text{Cu}^+/\text{Cu}$  is  $-0.350 \text{ V}$  at 353 K [61]. This phenomenon is attributed to the unique properties of DESs that provide different chemical environments for molecule solutions. Hence, the galvanic replacement reaction (GRR) between Cu and  $\text{Ni}^{2+}$  in ChCl/EG is thermodynamically feasible. This makes it possible to prepare Ni thin films on copper substrates by GRR. Using this theory, Zhang et al. prepared a series of nickel-based catalysts on the surface of copper foils (Figure 2b) [61]. Cu foils were put into ChCl/EG containing  $\text{NiCl}_2$ . At the beginning of the reaction, Cu foils released electrons that could be oxidized to  $\text{CuCl}_3^{2-}$ , accompanied by the appearance of surface cracks. Rough and porous surfaces of Cu foils were formed and then acted as templates for the Ni films. With the increase in immersion time,  $\text{Ni}^{2+}$  was gradually reduced to Ni nanocrystallites and deposited on Cu foil. Finally, self-supported three-dimensional (3D) nanoporous Ni films were obtained. The obtained Ni films exhibited high HER catalytic activity with a low overpotential of 170 mV to arrive at  $10 \text{ mA cm}^{-2}$  and a relatively small Tafel slope of  $98.5 \text{ mV dec}^{-1}$  in alkaline media.

Based on the above work [61], this group then synthesized  $\text{Ni}_3\text{S}_2@\text{Cu}$  using GRR through adding thiourea as well as Cu foil into a  $\text{ChCl}/\text{EG}-\text{NiCl}_2$  system [62]. When the replacement reaction occurred between Cu and  $\text{Ni}^{2+}$ , S was doped into Ni films to form S-doped Ni microsphere films on nanoporous Cu substrates (Figure 2c). It has been known that S can initiate structure changes with the superior exposed active position and electronic conductivity of Ni-based catalysts. Therefore, the addition of S could enhance the hydrogen evolution performance. The activated  $\text{Ni}_3\text{S}_2@\text{Cu}$  showed a high electrocatalytic HER activity with small Tafel slopes of 63.5 and 67.5  $\text{mV dec}^{-1}$  in acidic and alkaline media, respectively. It required  $\eta_{10}$  ( $\eta$  represents the overpotential,  $\eta_{10}$  is the overpotential corresponding to a current density of  $10 \text{ mA cm}^{-2}$ ) of 91.6 mV in 0.5 M  $\text{H}_2\text{SO}_4$  and 60.8 mV in 1.0 M KOH, respectively.  $\text{Ni}_3\text{S}_2@\text{Cu}$  exhibited higher catalytic activity than Ni nanocrystallites@Cu.

Similar to the preparation of nickel sulfides, nickel phosphides have been successfully prepared by adding appropriate P sources to DES-nickel salt systems using an ionothermal method [63], electrodeposition method [64,65], etc. The P-doped nickel films were formed on copper foil by electrodeposition in  $\text{ChCl}/\text{EG}$  containing a different Ni : P ratio (Figure 2d). The synergistic effect between P and Ni induced excellent HER catalytic performance. They could achieve  $\eta_{10} = 105 \text{ mV}$  with a small Tafel slope ( $44.7 \text{ mV dec}^{-1}$ ) when it had the suitable Ni:P ratio (1:0.056) [64].

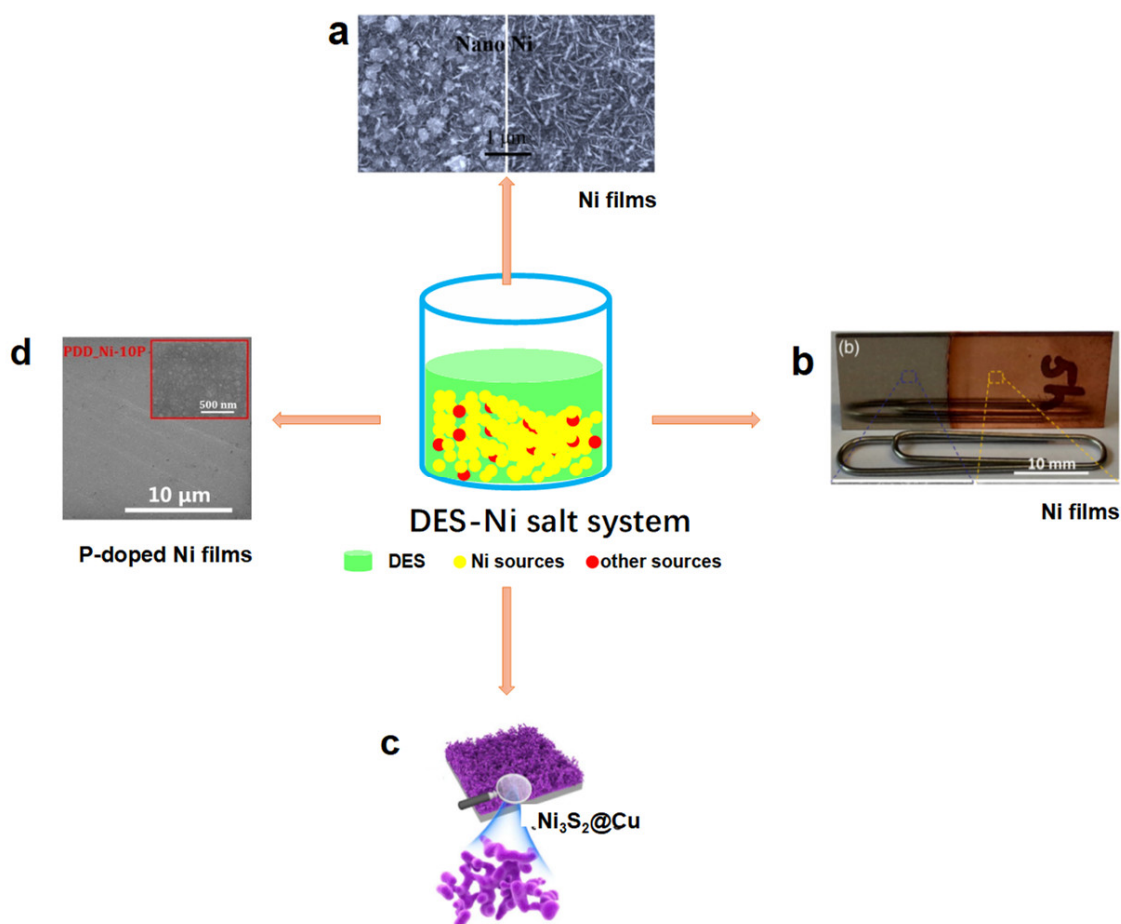


**Figure 2.** Electrochemical catalysts obtained from DES–Ni system: (a) Ni film. Reproduced with permission from ref. [57]. Copyright 2018 Elsevier. (b) Ni films. Reproduced with permission from ref. [61]. Copyright 2016 Elsevier. (c)  $\text{Ni}_3\text{S}_2@\text{Cu}$ . Reproduced with permission from ref. [62]. Copyright 2017 Elsevier. (d) P-doped Ni films. Reproduced with permission from ref. [64]. Copyright 2019 American Chemical Society.

The preparation of Ni-based bimetallic, even multimetallic, catalysts in DESs has drawn increasing attention. Adding the second metal salt, even several metal salts, into DES-nickel salt systems can produce Ni-based multimetallic nanomaterials, such as Ni-Mo/Cu [66], Ni-Mo-Cu [67], Ni-Cu [68], Ni-Co-Sn [69], Ni-Fe [70,71],  $\text{Co}_x\text{-Ni(OH)}_2/\text{Cu}$  foam [72],  $\text{NiCo}_2\text{O}_4$  [73],  $(\text{FeCoNiCuZn})(\text{C}_2\text{O}_4)\cdot 2\text{H}_2\text{O}$  [74], and so on. The Ni-based multimetallic combination will regulate the position of the d-band and the electronic structure of Ni, resulting in the superior kinetics, selectivity, and stability. Therefore, they are high-performance catalysts for HER and OER. Taking Ni-Mo/Cu as an example, it required a low HER overpotential of 63 mV to deliver  $20 \text{ mA cm}^{-2}$  with a small Tafel slope of  $49 \text{ mV dec}^{-1}$  [66]. It also offered excellent OER electrocatalytic activity with an overpotential of 335 mV to reach  $20 \text{ mA cm}^{-2}$ , as well as a moderated Tafel slope of  $108 \text{ mV dec}^{-1}$ . Furthermore, this catalyst needed a cell voltage of 1.59 V to achieve a current density of  $10 \text{ mA cm}^{-2}$  for overall  $\text{H}_2\text{O}$  splitting.

According to the preparation idea of metal sulfide, adding S sources into Ni-based bimetallic DES system will generate Ni-based bimetallic sulfides [75]. For example, adding thiourea into  $\text{ChCl}/\text{EG}$  containing  $\text{NiCl}_2\cdot 6\text{H}_2\text{O}$  and  $\text{FeCl}_3\cdot 6\text{H}_2\text{O}$  could synthesize 3D amorphous S-NiFe<sub>2</sub>O<sub>4</sub>/Ni<sub>3</sub>Fe films via the electrodeposition route [76]. It exhibited excellent OER catalytic activity with overpotentials of only 260 mV and 285 mV to deliver  $100 \text{ mA cm}^{-2}$  and  $500 \text{ mA cm}^{-2}$  in alkaline solution, respectively, which was equivalent to the reported Ni-S as well as Ni-Fe OER electrocatalysts at  $100 \text{ mA cm}^{-2}$ . Similarly,  $\text{ChCl}/\text{EG}$  involving  $\text{NiCl}_2$ ,  $\text{CoCl}_2$  and thiourea system drove a 3D hierarchically porous Co,S-co-modified nickel microsphere array to grow on nickel foam ( $\text{NiCo}_x\text{S}_y/\text{NF}$ ), still using electrodeposition technology [77]. The optimal  $\text{NiCo}_{0.2}\text{S}_{0.8}/\text{NF}$  required  $\eta_{20} = 65 \text{ mV}$  for HER as well as  $\eta_{20} = 270 \text{ mV}$  for OER in a 1.0 M KOH solution. Moreover, it could achieve overall  $\text{H}_2\text{O}$  splitting at 1.57 V with high durability.

DES-assisted cobalt-based catalysts for overall water splitting are also receiving attention. They are synthesized by the similar synthetic protocol to DES-mediated Ni-based catalysts [78]. Generally, in DESs containing cobalt sources, the addition of other reactants, such as  $\text{NaH}_2\text{PO}_2\cdot \text{H}_2\text{O}$  [79],  $\text{SeO}_2$  [80], thiourea [81,82],  $\text{NH}_4\text{VO}_3$  [83] and so on, can produce Co-P nanoparticles, Co-O/Co-Se hybrid films, Co-S films,  $\text{CoV}_2\text{O}_6$  nanocrystals, etc. The ratio of Co and heteroatom in DESs directly affects the catalytic performance. For example, when P:Co was 1:1, Co-P@NF showed lower overpotentials of 62 mV and 320 mV at  $10 \text{ mA cm}^{-2}$  for HER as well as OER, respectively [79]. In addition, experiments have found that DESs can make difficult-to-obtain electrocatalysts more accessible. In  $\text{ChCl}/\text{EG}$  DES, 3D pompom-like Co-O and Co-Se hybrid films anchored on copper foils (Co-O@Co-Se/Cu) were prepared via potentiostatic electrodeposition process [80]. The incorporation of Se induced an interesting morphological change with the nanoparticles' packed flat structure for the deposited Co/Cu (Figure 3a-c). The resulting high surface area and the porous architecture played key roles in significantly increasing the surface active sites and promoting the intrinsic catalytic activity. It has been known that cobalt-vanadium oxides are generally prepared through using vanadium oxides and cobalt salts by solid state reaction, hydrothermal or co-precipitation methods [84,85]. However, these approaches often require long synthesis time, high reaction temperature or result in amorphous products. Using DESs as the reaction media can overcome the above defects. The well-defined octahedral  $\text{CoV}_2\text{O}_6$  nanomaterials were synthesized from 1:1  $\text{ChCl}/\text{malonic acid}$  DES maline at a lower temperature [83], as shown in Figure 3d,e. This exhibited a high OER catalytic activity ( $\eta_{10} = 324 \text{ mV}$ ) with high durability for over 24 h (Figure 3f). Compared with the traditional solid state route, DES-assisted synthesis had two obvious advantages. Firstly, DES-assisted synthesis could be achieved at a lower reaction temperature. Researchers studied the generation mechanism of  $\text{CoV}_2\text{O}_6$  in DES in detail. The IR spectrum showed that at  $100^\circ\text{C}$ ,  $\text{CoCl}_2\cdot 6\text{H}_2\text{O}$  and  $\text{NH}_4\text{VO}_3$  first generated  $\text{MCl}_x^-$  in DESs, in which metal ions were mainly adsorbed by DES clusters. The hydrogen bond framework of the DES served as both a homogeneous medium and a template for metal ion stabilization. The crystals were then obtained by calcination. A non-identifiable crystalline

phase was observed at 400 °C. Increasing to 500 °C for 2 h obtained a clear crystalline phase of  $\alpha$ -CoV<sub>2</sub>O<sub>6</sub>. Obviously, DES-derived strategy obtained products at a lower temperature than the solid state route (typically a reaction condition of 720 °C for 40 h using vanadium oxide and hydrogenated cobalt oxide). It was found that the formation of DES-assisted CoV<sub>2</sub>O<sub>6</sub> began with the initial pyrolysis of maline initiated by metal salts. The reason was that the presence of Lewis acid of MCl<sub>x</sub>, especially CoCl<sub>2</sub>, could decrease the endo effect of the thermodestruction of DES, which initially triggered the thermal destruction of DES at an early stage. Light species obtained from the decomposition of DESs, such as CO, CO<sub>2</sub>, methane, ethane, etc., underwent further combustion with atmospheric oxygen, creating sufficient heat supply for oxide formation. The second advantage of a DES-assisted approach was that it could obtain well-defined octahedral morphology. This was because the supramolecular nature of the DESs, including hydrogen bonding and electrostatic interactions, reduced the overall energy required for phase formation. In addition, the added metal salt closely combined with the hydrogen bond network of maline to integrate the formed MCl<sub>x</sub> into the hydrogen bond solvent structure.

Since Fe element has a strong affinity for oxygen, the catalytic performance of Fe-based electrocatalysts is much lower than that of Ni- and Co-based materials. Fe is usually designed to be one of the components of multimetallic compounds. It is found that even a trace amount of Fe can reduce the overpotential of transition metal catalysts [86,87]. In 2014, Gu et al. synthesized CoFe layered double hydroxide (CoFe-LDH) with large layer spacing in ChCl/urea using a “water injection” method [88]. With the rapid injection of water, urea could be decomposed into OH<sup>-</sup>, which could react with Co and Fe ions to obtain CoFe-LDH. In this process, the derivative species from DES were used as intercalators, contributing to the formation of large distances of interlayers. The prepared CoFe-LDH had good OER performance. Using a similar method, this group also synthesized Ni(OH)<sub>2</sub> [89] and Co(OH)<sub>2</sub> [90]. Recently, with a facile one-step electrodeposition process performed in ChCl/urea DES, Zhang et al. fabricated an Fe-doped bimetallic phosphate electrocatalyst, directly grown on a Cu substrate [91]. In this system, the iron content could be flexibly adjusted. The optimized Fe-doped bimetallic phosphate electrocatalysts exhibited efficient HER catalytic performance in acidic, alkaline, and neutral solutions. In addition, the catalyst also exhibited excellent OER performance in alkaline conditions. The authors considered that the superior performance of the catalyst was reflected in two aspects. Firstly, doping of Fe could tailor O active electronic properties in phosphate. Secondly, the combination of the unique 3D microsphere structure with a two-dimensional (2D) nanosheet internal architecture provided enough active sites to favor transfer kinetics.

After all, iron is the most plentiful transition metal element in the Earth’s crust, while having the advantages of good physicochemical properties and high safety. The study of single Fe-based catalysts has been concerned with the electrolysis of water. Recently, high-performance Fe-based catalysts have been successfully prepared in DESs. FeS<sub>x</sub> films were fabricated via adding thiourea into ChCl/EG containing FeCl<sub>3</sub> 6H<sub>2</sub>O. This required 340 mV to produce 10 mA cm<sup>-2</sup> for OER [92]. Our group prepared DES-derived Fe<sub>7</sub>S<sub>8</sub>/Fe<sub>2</sub>O<sub>3</sub> via the reaction between Fe powder and thioacetamide in ChCl/glycerol (1:2) DES [93]. The 2D porous nanosheets were attributed to the structure-directing function of ChCl/glycerol. Annealing at 400 °C under a nitrogen atmosphere generated a large amount of oxygen vacancies and improved the crystallinity of products. Under the synergistic effect of Fe<sub>7</sub>S<sub>8</sub> and Fe<sub>2</sub>O<sub>3</sub>, it only required a low overpotential of 229 mV to produce a current density of 10 mA cm<sup>-2</sup> for OER, while processed low Tafel slope of 49 mV dec<sup>-1</sup> in 1.0 M KOH.

Metal Mn has increasingly attracted attention. Zhang’s group generated S-MnO<sub>x</sub>/Mn through electrodeposition and in situ electrochemical oxidation (Figure 3g–l) [94]. Compared with traditional aqueous solutions, DES has unique solvent characteristics, including low water activity, wide electrochemical window, highly ordered hydrogen bonds and large surface tension. These characteristics produced self-supporting Mn nano sheet arrays on carbon paper conductive substrates. Doping of S could change the phase composition and electronic structure of this catalyst, offering a highly porous architecture with plentiful

exposed edges, while the electro-oxidation led to tailored phase composition. The introduction of S improved the catalytic performance. In addition, the perfect combination of  $\text{MnO}_x$  (high activity) and Mn (high conductivity) was conducive to reaction kinetics and electron transfer. As a result, S-MnO<sub>x</sub>/Mn offered a low overpotential ( $\eta_{10} = 435$ ) with a Tafel slope of  $89.97 \text{ mV dec}^{-1}$ .

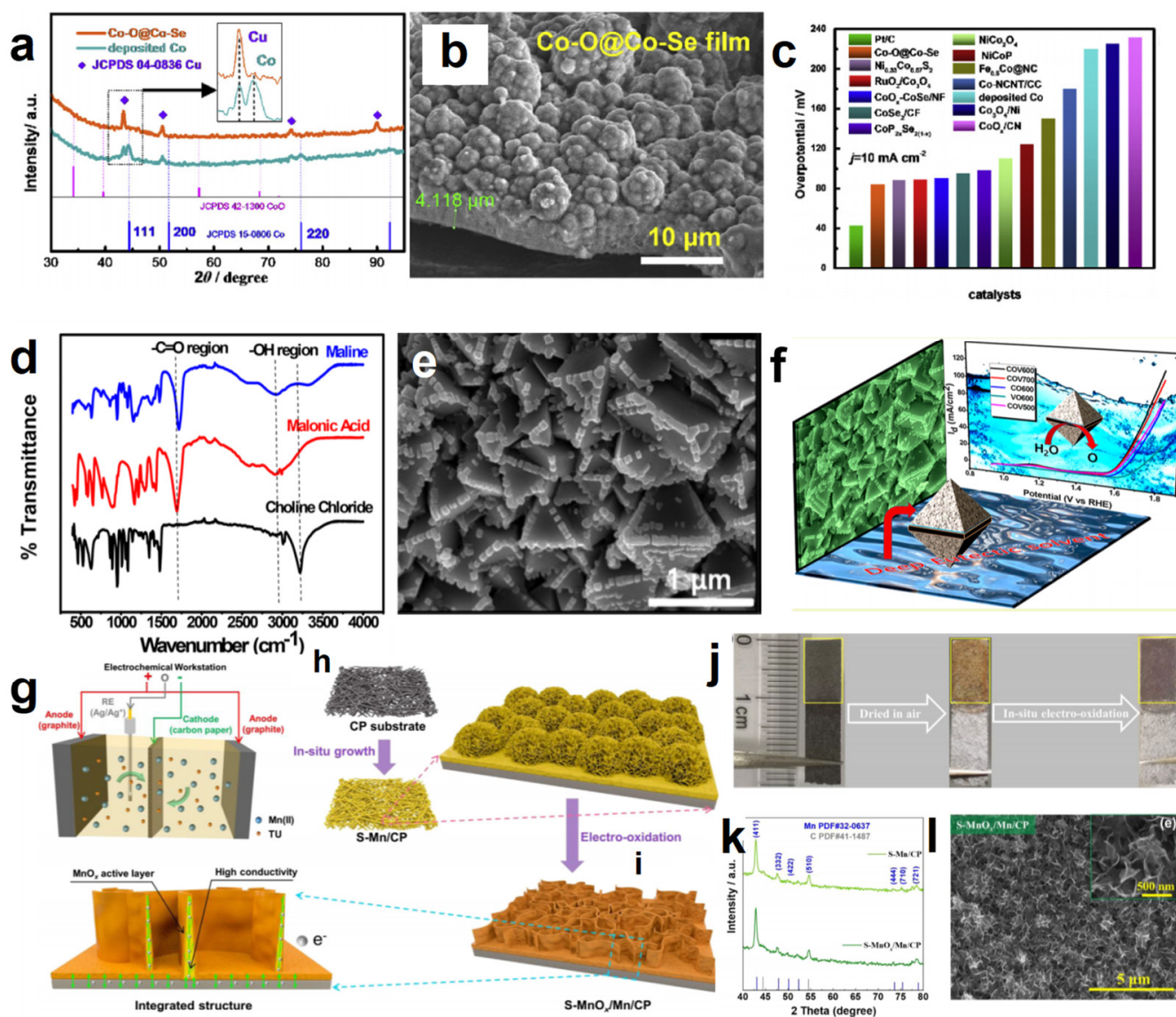


**Figure 3.** XRD patterns of Co-O/Co-Se (a), the cross section of the Co-O/Co-Se (b), comparison of the required potential at  $10 \text{ mA cm}^{-2}$  for the Co-O/Co-Se/Cu with other cobalt-based HER electrocatalysts (c). Reproduced with permission from ref. [80]. Copyright 2018 Elsevier; The IR spectrum of ChCl, malonic acid, and ChCl/malonic acid, respectively (d), SEM of CoV<sub>2</sub>O<sub>6</sub> calcinated at 600 °C (e), diagram of octahedral CoV<sub>2</sub>O<sub>6</sub> and its corresponding OER performance (f). Reproduced with permission from ref. [83]. Copyright 2018 American Chemical Society; Schematic of the three-electrode system for the preparation of active phases (g), direct growth of S-Mn nanoflake arrays in DES (h), in situ electrochemical oxidation to form S-MnO<sub>x</sub>/Mn (i), the optical image of preparation process of S-MnO<sub>x</sub>/Mn (j), XRD patterns (k) and SEM image (l) of S-MnO<sub>x</sub>/Mn. Reproduced with permission from ref. [94]. Copyright 2022 Elsevier.

Perovskites have attracted great interest as energy conversion materials due to their stability and structural tunability. Scientists have investigated a route to synthesize La-based perovskites using an environmentally friendly DES consisting of ChCl and malonic acid [95]. This method provided gram-scale and phase-pure crystalline materials and yielded high electrical active perovskites for the catalytic OER. Compared with perovskites prepared by other methods, the high activity of DES-derived LaCoO<sub>3</sub> was attributed to the high concentration of the oxygen vacancy lattice, exhibiting current densities of 10, 50, and 100 mA cm<sup>-2</sup> at corresponding overpotentials of approximately 390, 430, and 470 mV, respectively, and possessing a Tafel slope of 55.8 mV dec<sup>-1</sup>.

In addition to transition metal electrocatalysts, the DES-mediated noble metal (Pt, Rh, Ir, Ru et al.) electrocatalysts have also been studied [96]. They possess attractive properties, such as corrosion resistance, high conductivity and excellent electrocatalytic activity, making them ideal for applications. However, their application is limited by rare reserves and expensive value. Therefore, it is necessary to improve the efficiency of noble metals, such as by depositing precious metals on substrate. Pd was successfully attached to treated porous Ag surfaces (Pd@Ag), using ChCl/EG DESs containing PdCl<sub>2</sub> as a solvent by GRR [97]. The DES could provide a unique solvent environment and reaction kinetics, which made a potential difference between Pd<sup>2+</sup>/Pd (0.951V) and Ag<sup>+</sup>/Ag (0.799V) and enabled Pd to grow on the porous Ag surface controllably. Then Pt was deposited on Pd@Ag by the electrodeposition method to generate Pt-Pd@Ag, which had wonderful HER performance in acidic, alkaline and neutral solutions.

Ru is an important platinum group metal. Ru films are usually prepared by electrodeposition. However, the electrolyte required for electrodeposition of metal Ru films is generally a toxic cyanide-based electrolyte. The overlapping of metal ion reduction and solvent reduction during electrolysis promotes the deposition of ethoxylated products on surfaces. In order to solve the above problems, Lee et al. successfully synthesized Ru nanoparticles with a rough surface using ChCl/urea DES as the electrolyte and stainless steel mesh as the substrate. DES could dissolve metals well without any additives [98]. The prepared Ru films had excellent onset potential (27.3 mV) and Tafel slope (97 mV/dec) for HER equivalent to standard Pt electrocatalyst [99].

It can be seen from the above achievements that the catalysts can be conveniently obtained by adding an appropriate source of heteroatoms via appropriate synthesis techniques. This simple design enables the realization of catalysts with multiple components. The synergistic effect between different components can tailor the structure of catalysts, improve their electronic structure, and thereby improving the catalytic activity.

In addition to the synthesis of metal nanomaterials in DESs, DESs can also be used to exfoliate layered catalysts. Layered compounds are an effective class of energy conversion catalysts due to a great deal of exposed edge sites on 2D nanomaterials [100,101]. However, these active sites tend to be less active due to aggregation by electrostatic and coordination interactions. An exfoliation technique is often used to increase and stabilize the edge active sites so that they enhance the electrocatalytic activity. DESs are found to be an ideal exfoliation agent because of the species in DESs, such as ammonium ions, which can be inserted into the layered crystals by some shear forces [102–104]. Assisted by DESs, single- or few-layer 2D materials can be obtained through mechanical grinding or chemical methods. The reactions between ammonium ions and layers result in forming a charged layered sheet that significantly weakens the Van der Waals force. The layered sheets no longer hold together and disperse as individual thin sheets in the solution. MoS<sub>2</sub> is one of the typical layered compounds, which possesses a sandwich-like S–Mo–S layered structure stacked together via Van der Waals force. Mohammadpour studied the influence of DES composition on MoS<sub>2</sub> stripping effect (Figure 4a–f) [105]. A series of sugar-based natural DESs and ChCl-based DESs were employed as intercalating agents. Natural DESs refer to ingredients that are abundant natural metabolites (including sugars, amino acids or organic acids). It was found that sugar-based natural DESs could strip MoS<sub>2</sub>, whereas most ChCl-based DESs were unsuccessful in inducing nanosheet production. Further

comparing the stripping effect of different natural DESs, it was revealed that the natural DES of sucrose was better than that of either fructose or glucose. The reason was that sucrose-based DESs possessed larger molecular size than that from either fructose or glucose. Sucrose-based DESs formed large solvent clusters through hydrogen bonding. They could induce greater steric hindrance and were more prone to suppress the weak van der Waals interactions than those DESs involving smaller sized molecular components, when diffusing between the MoS<sub>2</sub> layers and exfoliating them. As intercalating agents as well as environmentally friendly solvents, naturally sourced and nontoxic sugar-based natural DESs were firstly reported to achieve the exfoliation of MoS<sub>2</sub> nanosheets with high yield. This study is likely to be extended to industry. The electrochemical testing results showed that the obtained 2H-1T MoS<sub>2</sub> nanosheets exhibited an overpotential of 339 mV at the current density of 10 mA cm<sup>-2</sup> and a long-term durability (2000 cycles) in acidic media for HER (Figure 4g,h). Subsequently, water was found to have the ability to modulate the molecular arrangement of DESs, inducing further regulating efficiency in MoS<sub>2</sub> [106].

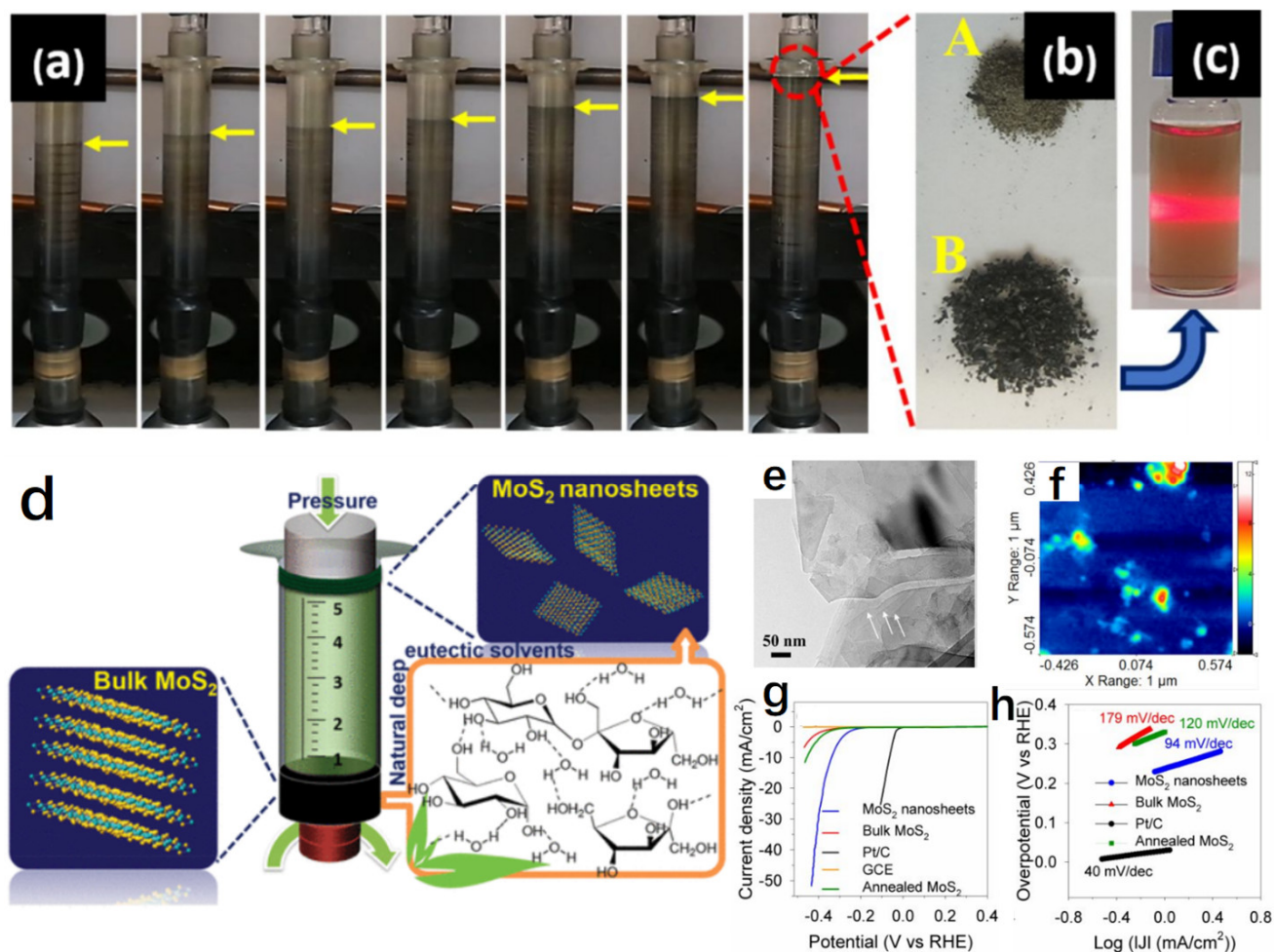


**Figure 4.** Longitudinal and gradual movement of the NADES/MoS<sub>2</sub> mixture toward the syringe flange over time (a), photos of the raw exfoliation products (b), tyndall scattering of the raw exfoliation products (c), schematic diagram of MoS<sub>2</sub> nanosheets synthesis process (d), TEM (e) and AFM (f) images of MoS<sub>2</sub> nanosheets, polarization curves (g) and Tafel plots (h) of MoS<sub>2</sub> nanosheets and other catalysts. Reproduced with permission from ref. [105]. Copyright 2018 American Chemical Society.

Table 2. Summary of HER, OER and Water Splitting Performance of Catalysts Involved in Section 2.

Catalyst	Applied DES	Preparation Method	Catalytic Performance								Ref.
			HER			OER			Water Splitting		
			Electrolyte	$\eta$ (mV)@ Current Density (mA cm <sup>-2</sup> )	Tafel Slope (mV dec <sup>-1</sup> )	Electrolyte	$\eta$ (mV)@ Current Density (mA cm <sup>-2</sup> )	Tafel Slope (mV dec <sup>-1</sup> )	Electrolyte	Potential (V)@ Current Density (mA cm <sup>-2</sup> )	
Ni	ChCl/Urea	Electrodeposition	1 M KOH	153@30	185	—	—	—	—	—	[57]
Ni/TiO <sub>2</sub>	ChCl/EG	Electrodeposition	1 M NaOH	—	122	—	—	—	—	—	[58]
Ni/Ni(OH) <sub>2</sub>	ChCl/EG	Electrodeposition	1 M KOH	110@10	83.9	1 M KOH	290@10	120.9	—	—	[59]
NiS <sub>x</sub>	ChCl/EG	Electrodeposition	1 M KOH	54@10	54	—	—	—	—	—	[60]
Ni	ChCl/EG	GRR	1 M KOH	170@10	98.5	—	—	—	—	—	[61]
Ni <sub>3</sub> S <sub>2</sub>	ChCl/EG	GRR	1 M KOH	60.8@10	67.5	—	—	—	—	—	[62]
Ni <sub>3</sub> S <sub>2</sub>	ChCl/EG	GRR	0.5 M H <sub>2</sub> SO <sub>4</sub>	63.5@10	91.6	—	—	—	—	—	[62]
NiP <sub>x</sub>	ChCl/EG	Electrodeposition	1 M KOH	105@10	44.7	—	—	—	—	—	[64]
Ni–P	ChCl/EG	Electrodeposition	1 M KOH	105@50	72.9	—	—	—	—	—	[65]
Ni–Mo	ChCl/EG	Electrodeposition	1 M KOH	63@20	49	1 M KOH	335@20	108	1 M KOH	1.59@10	[66]
Ni–Mo–Cu	ChCl/Urea	Electrodeposition	1 M KOH	93@10	105	—	—	—	—	—	[67]
Ni–Cu	ChCl/EG	Electrodeposition	1 M KOH	128@10	57.2	—	—	—	—	—	[68]
Ni–Co–Sn	ChCl/EG	Electrodeposition	1 M KOH	—	121	—	—	—	—	—	[69]
Ni–Fe	ChCl/EG	Electrodeposition	0.1 M KOH	316@10	62	—	—	—	—	—	[70]
Ni–Fe	ChCl/Urea	Electrodeposition	0.5 M NaOH	256@10	140.1	0.5 M NaOH	406@10	84.4	—	—	[71]
Co <sub>x</sub> –Ni(OH) <sub>2</sub>	ChCl/EG	Electrodeposition	1 M KOH	106@10	98.2	1 M KOH	330@100	126.7	—	—	[72]
NiCo <sub>2</sub> O <sub>4</sub>	ChCl/Glycerol Polyethylene glycol (PEG)/Oxalic acid	Calcining method	—	—	—	1 M KOH	320@10	67	—	—	[73]
(FeCoNiCuZn)(C <sub>2</sub> O <sub>4</sub> )· 2H <sub>2</sub> O	—	Ionothermal method	—	—	—	1 M KOH	334@10	67.93	—	—	[74]
NiCo <sub>x</sub> S <sub>y</sub>	ChCl/EG	Electrodeposition	1 M KOH	65@10	62.5	1 M KOH	300@20	109	1M KOH	1.57@10	[75]
S–NiFe <sub>2</sub> O <sub>4</sub> /Ni <sub>3</sub> Fe	ChCl/EG	Electrodeposition	—	—	—	1 M KOH	260@10	35	1 M KOH	1.52@10	[76]
NiCo <sub>x</sub> S <sub>y</sub>	ChCl/EG	Electrodeposition	1 M KOH	65@20	54	1 M KOH	270@20	35	1 M KOH	1.57@10	[77]
Co	ChCl/Malonic acid	Electrodeposition	—	—	—	1 M KOH	350@10	76	—	—	[78]
P–Co	ChCl–EG	Electrodeposition	1 M KOH	65@10	69.2	1 M KOH	320@10	91.15	1 M KOH	1.59@10	[79]
Co–O/Co–Se	ChCl/Urea	Electrodeposition	1 M KOH	85@10	71.9	1 M KOH	340@10	67.6	1 M KOH	1.65@10	[80]
Co–S	ChCl/EG	Electrodeposition	1 M KOH	59@10	65	1 M KOH	307@50	66.4	1 M KOH	1.69@50	[81]
CoS <sub>x</sub>	Ethanedithiol/ <i>n</i> – Butylamine	CO <sub>2</sub> –assited solution–processed method	—	—	—	1 M KOH	302@10	64.8	—	—	[82]
CoV <sub>2</sub> O <sub>6</sub>	ChCl/Malonic acid	Calcining method	—	—	—	1 M KOH	324@10	—	—	—	[83]
CoFe–LDH	ChCl/Urea	Water injection method	—	—	—	0.5 M KOH	Onset overpotential 510	—	—	—	[88]

Table 2. Cont.

Catalyst	Applied DES	Preparation Method	Catalytic Performance								Ref.
			HER			OER			Water Splitting		
			Electrolyte	$\eta$ (mV)@ Current Density (mA cm <sup>-2</sup> )	Tafel Slope (mV dec <sup>-1</sup> )	Electrolyte	$\eta$ (mV)@ Current Density (mA cm <sup>-2</sup> )	Tafel Slope (mV dec <sup>-1</sup> )	Electrolyte	Potential (V)@ Current Density (mA cm <sup>-2</sup> )	
Fe <sub>x</sub> Co <sub>3-x</sub> (PO <sub>4</sub> ) <sub>2</sub>	ChCl/Urea	Electrodeposition	1 M KOH	108.1@100	30.3	1 M KOH	310@10	40.2	1 M KOH	1.62@10	[91]
Fe <sub>x</sub> Co <sub>3-x</sub> (PO <sub>4</sub> ) <sub>2</sub>	ChCl/Urea	Electrodeposition	0.5 M H <sub>2</sub> SO <sub>4</sub>	128.8@100	42.4	—	—	—	—	—	[91]
Fe <sub>x</sub> Co <sub>3-x</sub> (PO <sub>4</sub> ) <sub>2</sub>	ChCl/Urea	Electrodeposition	1 M Phosphate- buffered saline (PBS)	291.5@100	117.6	—	—	—	—	—	[91]
FeS <sub>x</sub>	ChCl/EG	Electrodeposition	—	—	—	1 M KOH	340@10	—	—	—	[92]
Fe <sub>7</sub> S <sub>8</sub> /Fe <sub>2</sub> O <sub>3</sub>	ChCl/glycerol	Calcining method	—	—	—	1 M KOH	229@10	49	—	—	[93]
S-MnO <sub>x</sub> /Mn	ChCl/EG	Electrodeposition and in-situ electrochemical oxidation	—	—	—	1 M KOH	435@10	89.97	—	—	[94]
LaCoO <sub>3</sub>	ChCl/Malonic acid	Calcining method	—	—	—	1 M NaOH	390@10	55.8	—	—	[95]
Pt-Pd@Ag	ChCl/EG	GRR and Electrodeposition	0.5 M H <sub>2</sub> SO <sub>4</sub>	28.1@10	31.2	—	—	—	—	—	[97]
Pt-Pd@Ag	ChCl/EG	GRR and Electrodeposition	1.0 M PBS	34.8@10	32.2	—	—	—	—	—	[97]
Pt-Pd@Ag	ChCl/EG	GRR and Electrodeposition	1 M KOH	23.8@10	32.5	—	—	—	—	—	[97]
Ru	ChCl/urea	Electrodeposition	0.5 M H <sub>2</sub> SO <sub>4</sub>	65.7@10	97	—	—	—	—	—	[99]
MoS <sub>2</sub>	A series of sugar-based natural DESs	Mechanical stirring	—	—	—	0.5 M H <sub>2</sub> SO <sub>4</sub>	339@10	94	—	—	[105]

### 3. Deep Eutectic Solvents as Reactive Reagents of Metal Electrocatalysts for HER and OER

The designability of DESs has prompted more enthusiasm to design them as active components which directly participate in forming catalysts [107]. This synthesis strategy has the following advantages. (1) DESs serve simultaneously as media, templates and reactants, making the reaction systems simple and reproducible. Meanwhile, the strategy which directly uses DESs as reagents is expected to realize 100% conversion of reactants. (2) HBDs and/or HBAs in DESs can be decomposed to release small molecules or ionic groups under appropriate stimulation, providing S, P, N, C, and even metal elements. Compared with traditional phosphorus and sulfur sources, and so on, DESs as heteroatom sources possess safety, green advantages, and other special properties. (3) The supramolecular structures of DESs have inheritance characteristics, which shape the structures and tune the performance of catalysts. Many kinds of DES-derived electrocatalysts, including metal-based catalysts, N-doped carbon materials, and metal and heteroatom co-doped carbon materials, have been synthesized and exhibited high performance (Table 2) by means of DESs as active species [108].

#### 3.1. Deep Eutectic Solvents as Heteroatom Sources to Prepare Metal Electrocatalysts

The combination of metal and nitrogen-doped porous carbon is an effective strategy to improve the activity and stability of catalysts due to the improvement of conductivity [109,110]. Urea is an ideal nitrogen source for preparing N-containing catalysts [111]. Glucose, one of the most important and widely distributed compounds in nature, is a promising sustainable resource due to non-toxicity, renewability and low cost [112,113]. Glucose-based natural DESs are commonly used as precursors to prepare carbonaceous materials by heating DESs under  $N_2$ . Pyrolysis of glucose/urea DES under a  $N_2$  atmosphere can produce 2D N,O-doped graphene [114]. Experimental results demonstrated that the DES calcining method was a comprehensive approach to produce novel carbon materials and adjust product morphology [115]. Furthermore, adding metal precursors into glucose/urea, DES could produce carbon flakes loaded with metal species via calcining them together without air, in which graphene flakes formed from DES acted as templates. When the products were further calcined under air, the graphene templates were removed. A series of metal oxides, such as  $La_{0.5}Sr_{0.5}Co_{0.8}Fe_{0.2}O_3$ ,  $Co_3O_4$ ,  $NiCo_2O_4$ ,  $RuO_2$  and  $Ba_{0.5}Sr_{0.5}Co_{0.8}Fe_{0.2}O_3$ , were formed with low-dimensional hierarchical porous structure because graphene flakes formed from DES acted as template. These transition metal oxides could be applied for the OER.  $La_{0.5}Sr_{0.5}Co_{0.8}Fe_{0.2}O_3$  had the highest OER electrocatalytic activities (304 mV overpotential at a current density of  $10 \text{ mA cm}^{-2}$ ). Li further added  $ChCl$  to glucose/urea DES, obtaining  $ChCl$ /urea/gluconic acid ternary DES [116]. Cobalt nanoparticles supported on N-doped porous carbon (Co@NPC) were in situ synthesized through one-pot pyrolysis of this ternary DES and  $Co(NO_3)_2 \cdot 6H_2O$ . Co@NPC was employed as a bifunctional electrocatalyst for simultaneous HER and glucose oxidation reaction, a reaction instead of OER to promote  $H_2$  generation. Using urea or glucose components of DESs to provide N or C species is more effective than using pure urea or glucose. Firstly, DES ensures significant nitrogen contents due to the uniform incorporation of nitrogen into the solution phase of the synthesis process. Secondly, DES acts as a self-template to form an integral hierarchical structure composed of highly cross-linked clusters.

Our research group has engaged in in depth research to synthesize inorganic nanomaterials using DESs as reactive reagents. We rationally prepared DES-derived iron alkoxide based on the following considerations [117]. Firstly, it is found that the catalysts can slowly self-optimize under the condition of water electrolysis. Their structure and composition are transformed in situ [118]. Therefore, many reports have demonstrated the conversion of Fe-based catalysts during OER process. For example, tannic acid-nickel iron [119], FeSe vertical nanosheet array [120], etc., converted into  $FeOOH$ , a genuine active intermediate for electrocatalysis. Inspired by these achievements, we wonder whether iron alkoxide can catalyze water splitting and be converted to  $FeOOH$  under alkaline conditions, eliminating the

steps to prepare FeOOH beforehand. Secondly, the preparation involving DESs is expected to shape special structures. The resulting product should be different from pure glycerol as a reactant as well as a medium. To explore the above problems, we chose ChCl/glycerol (1:2) as a benign reaction medium, in which glycerol was not only HBD but also the reactant [31]. After  $\text{Fe}(\text{NO}_3)_3$  was put into ChCl/glycerol, a hydrogen bond was generated between  $\text{NO}_3^-$  and  $\text{C}_3\text{H}_8\text{O}_3$ , while  $\text{Fe}^{3+}$  was strongly chelated by  $\text{C}_3\text{H}_8\text{O}_3$ . Thus,  $\text{Fe}(\text{NO}_3)_3$  was easy to integrate into chcl/glycerol by hydrogen bonds as well as coordination bonds. Then the hierarchically 3D Fe-based organic-inorganic hybrid microspheres (Fe\_DES) with large surface area was obtained at  $150^\circ\text{C}$  for 11 h via solvothermal method (Figure 5a–d). Compared with pure glycerol, Fe\_DES had superior structure and properties to the product from glycerol (Fe\_Gly), which was amorphous and irregular. This stems from the special structure and properties of DES. The catalytic performance of Fe\_DES was better than that of Fe\_Gly. The overpotentials of Fe\_DES only needed 280 mV and 300 mV to obtain  $10\text{ mA cm}^{-2}$  and  $20\text{ mA cm}^{-2}$ , respectively, while the Tafel slope was small with good stability (Figure 5e–h). As expected, the oxygen evolution activity of Fe\_DES improved significantly from the 1st to 40th indicated by the polarization curves. After 40 cycles, a stable polarization curve was reached. This activation process was attributed to its change in chemical composition and morphology in the alkaline electrolyte. It was found that the as-synthesized iron alkoxide was transformed into FeOOH during catalyzing of OER. The formation of FeOOH in situ afforded a sustainable catalytic performance. Meanwhile, the structure was reconstructed to a wrinkled surface which was more favorable than the original morphology, although basically maintaining the original microspheres and size (Figure 5i,j). The work has several innovations, including (1) developing a new method to prepare alkoxides, (2) firstly discovering iron alkoxide as a novel type of OER catalyst, (3) offering a guideline for the reasonable design of transformation-based catalysts in situ.

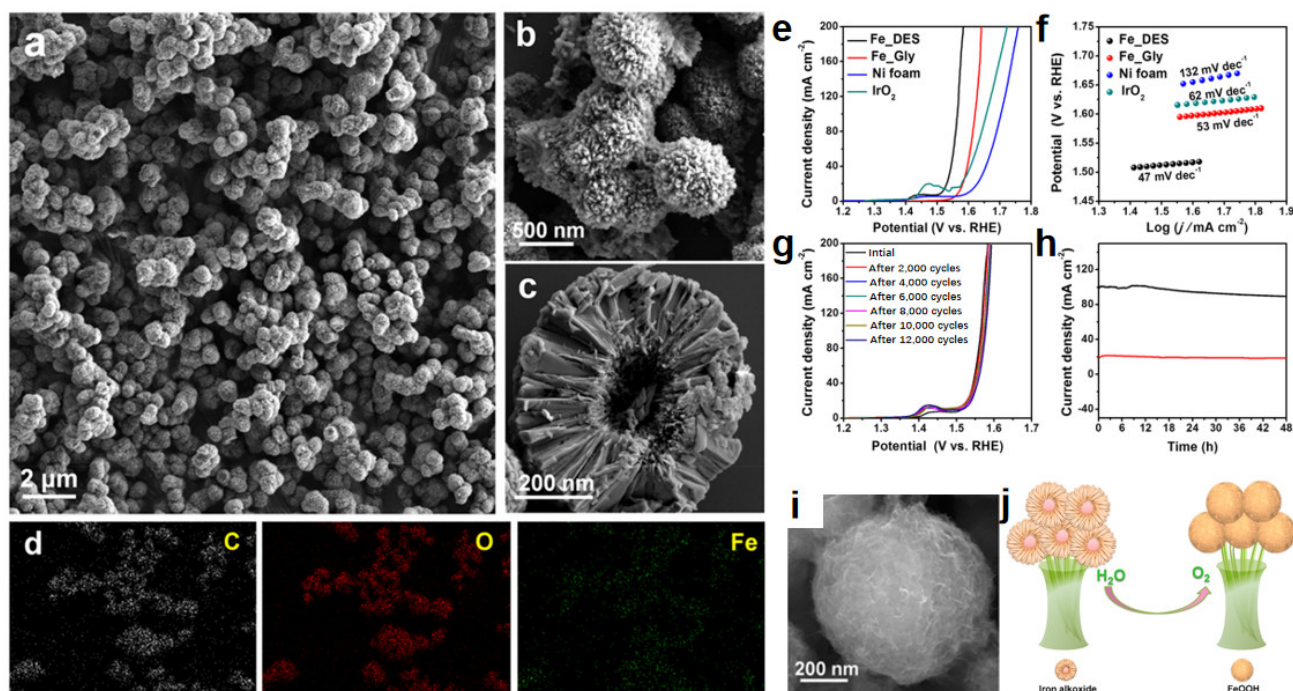


**Figure 5.** SEM images of low and high magnification (a–c) and EDX mapping (d) of iron alkoxide (Fe\_DES), polarization curves (e), Tafel plots (f), polarization curves before and after cyclic voltammogram treatment (g), and chronoamperometry study (h) of Fe\_DES, respectively. SEM image of Fe\_DES after OER reaction (i), schematic illustration for the conversion from iron alkoxide to FeOOH during the OER process (j). Reproduced with permission from ref. [117]. Copyright 2019 American Chemical Society.

The participation of DESs can alter the conventional synthetic routes. The traditional preparation of metal sulfides usually requires a two-step method. Metal (hydro)oxides are preferentially prepared. Then they are vulcanized through adding sulfide sources [121,122]. This process is not only complicated but also poorly reproducible. The designability of DESs offers the possibility for simply synthesizing metal sulfides. Mu et al. devised a novel polyethylene glycol (PEG) 200/thiourea DES to prepare sulfides via a one-step solvothermal method [123,124]. Good solubility of DES in various metal salts led to a series of transition metal sulfides, such as  $\text{CoS}_2$ ,  $\text{NiS}_2$ ,  $\text{Fe}_3\text{S}_4$  and  $\text{Ni}_2\text{CoS}_4$ , to be synthesized by adding metal salts to this PEGylated DES. As a multifunctional DES, the PEGylated DES acted as a solvent, shape-control agent and S source. Compared with traditional sulfuration approaches, this strategy was both economical and energy-saving by combining the solvothermal synthesis with the sulfuration process. The obtained  $\text{NiCo}_2\text{S}_4$  exhibited a spherical sea urchin-like micro-/nano-structure composed of uniformly interconnected nanorods. It also showed a high surface area, abundant active sites, easy diffusion of electrolytes and oxygen gas, and strong structural integrity. Consequently,  $\text{NiCo}_2\text{S}_4$  exhibited excellent OER properties. The overpotential was 337 mV to achieve  $10 \text{ mA cm}^{-2}$  with the Tafel slope of  $64 \text{ mV dec}^{-1}$  in 1.0 M KOH. Furthermore,  $\text{NiCo}_2\text{S}_4$  presented long-term durability with little inactivation after 2000 cycles of successive operations.

From the achievements mentioned above, we know that DESs can participate in the reaction through their own decomposition. However, metals, as the central components of catalysts, would still need to be added in addition. To further simplify the synthesis process and achieve uniformity of element distribution, metal sources can also be designed as compositions of DESs. Hydrated metal chloride-based Type IV DESs have drawn great attention.

### 3.2. Hydrated Metal Chloride-Based Deep Eutectic Solvents as Metal Sources to Prepare Metal Electrocatalysts

Hydrated metal halide-based DESs are an important class of DES [125]. There are not only hydrogen bonds but also coordination between metal ions and oxygen donor ligands in DESs. They have special liquid structures.  $\text{NiCl}_2 \cdot 6\text{H}_2\text{O}$ -based DESs have always been the focus of research.  $\text{NiCl}_2 \cdot 6\text{H}_2\text{O}$  as HBA is often paired with carbon-rich HBD to form a DES, such as  $\text{NiCl}_2 \cdot 6\text{H}_2\text{O}/\text{PEG 200}$ ,  $\text{NiCl}_2 \cdot 6\text{H}_2\text{O}/\text{malonic acid}$  and so on. They can provide both nickel and carbon species [126–128]. By sulfurizing or phosphating these kinds of DESs, carbon hybridized nickel sulfides or nickel phosphides are obtained. When  $\text{NiCl}_2 \cdot 6\text{H}_2\text{O}/\text{PEG 200}$  DES reacted with sublimed sulfur, a 2D  $\text{NiS}/\text{graphene}$  heterostructure was obtained via pyrolysis accompanied by sulfuration process in the tube furnace (Figure 6a,b) [126]. The ratio of graphene to  $\text{NiS}/\text{graphene}$  was tailored by simply changing the amount of PEG 200. In this kind of preparation strategy, both HBA and HBD participate in the reaction as reaction components, achieving the complete conversion of DESs. More importantly, the one-step procedure favored the interface coupling between graphene and  $\text{NiS}$  nanosheets, which significantly enhanced the electrical conductivity. The as-obtained  $\text{NiS}/\text{graphene}$  manifested excellent HER as well as OER activity in an alkaline solution. Furthermore, it showed a low cell voltage of 1.54 V at  $10 \text{ mA cm}^{-2}$ , superior to the integrated  $\text{IrO}_2$  and Pt/C couples for water splitting. Similarly, the graphene oxide coated  $\text{NiS}_2$  ( $\text{NiS}_2@\text{GO}$ ) was obtained via pyrolysis of the mixture of  $\text{NiCl}_2 \cdot 6\text{H}_2\text{O}/\text{malonic acid}$  DES and sublimed sulfur (Figure 6c–f). The unique DES supramolecular structure was conducive to the in situ growth of graphene in  $\text{NiS}_2$ , and promoted the formation of gas channels. Optimized  $\text{NiS}_2@\text{GO}$  catalysts required  $\eta_{10} = 57 \text{ mV}$  and 294 mV toward HER and OER in an alkaline solution, respectively. Meanwhile, the battery voltage of 1.52 V could be obtained with being stable for 48 h. The excellent performance of water splitting may be attributed to the following aspects: (1) The interaction between different interfaces was conducive to the transmission of electrons; (2) The electrons of the catalysts could penetrate the shell films of GO to enhance the electrocatalytic reaction; (3) GO shell films could effectively protect  $\text{NiS}_2$  nanospheres from corrosion and prevent  $\text{NiS}_2$  from spreading out during electrolysis,

inducing long-term stability and durability [127]. Ni<sub>2</sub>P@graphene was obtained through phosphating NiCl<sub>2</sub>·6H<sub>2</sub>O/malonic acid using NaH<sub>2</sub>PO<sub>2</sub>·2H<sub>2</sub>O [128]. It exhibited excellent activity with the potential of 1.51 V to arrive at 10 mA cm<sup>-2</sup> for overall water splitting.

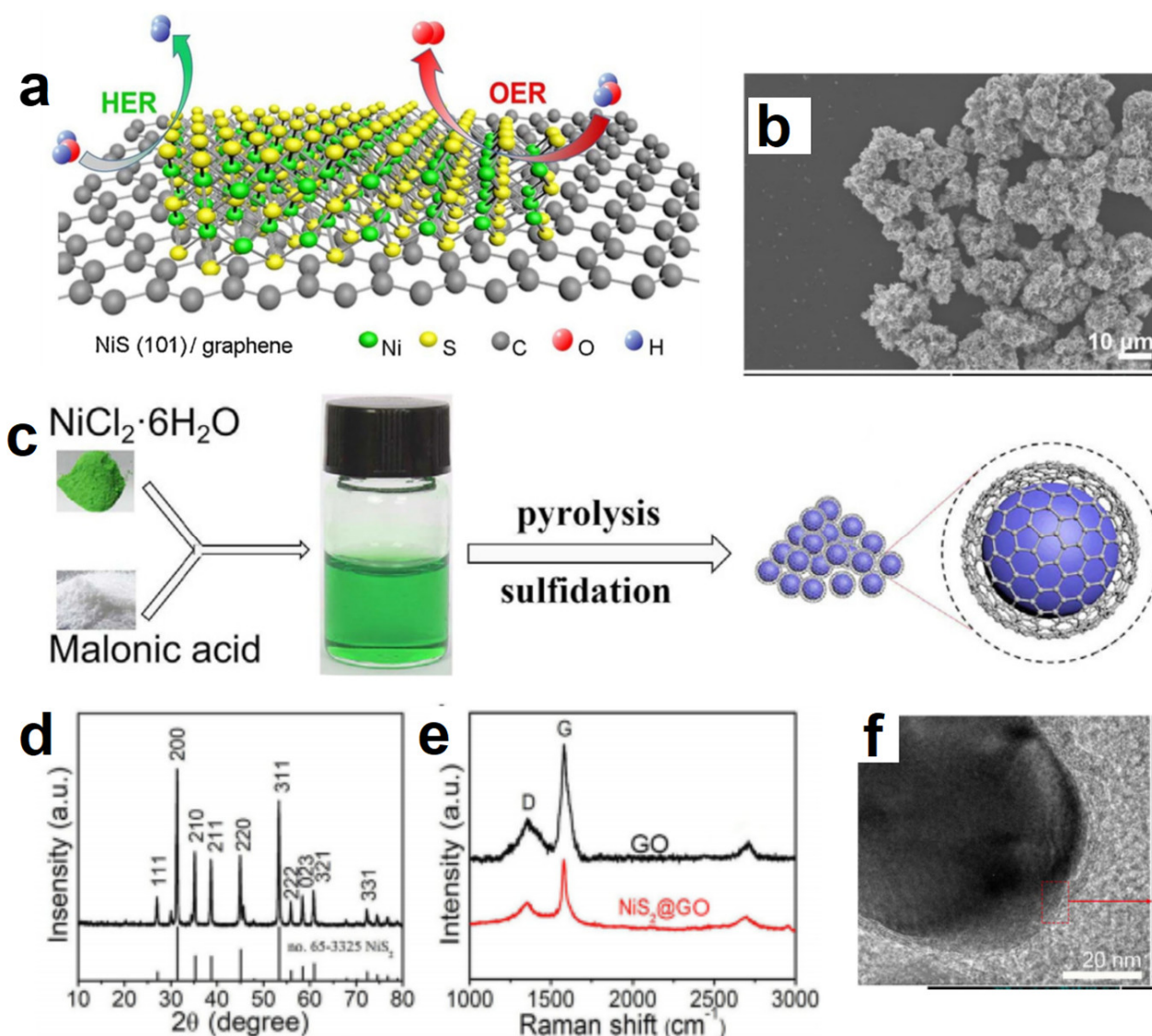


**Figure 6.** Schematic diagram of 2D NiS/graphene (a), SEM image of 2D NiS/graphene (b). Reproduced with permission from ref. [126]. Copyright 2019 Elsevier. Diagram of synthesis process and the microstructure of NiS<sub>2</sub>@GO (c); XRD pattern (d), Raman spectra (e) and TEM image (f) of NiS<sub>2</sub>@GO. Reproduced with permission from ref. [127]. Copyright 2020 Elsevier.

Metal halides and urea can also form a series of interesting DESs [129]. These kinds of DESs can introduce N, C, and metal elements into the catalysts. Based on this system, adding sulfur or phosphorus sources can produce N, C-co-doped catalysts by pyrolysis. For example, adding S source to NiCl<sub>2</sub>·6H<sub>2</sub>O/urea could produce 2D N-C/NiS<sub>2</sub> nanosheets through sulfuration, which exhibits enhanced catalytic performance for water splitting [129].

Compared with NiCl<sub>2</sub>·6H<sub>2</sub>O, FeCl<sub>3</sub>·6H<sub>2</sub>O-based DESs as an iron source have less attention paid to them than synthesizing Fe-based micro/nanomaterials. To understand the behavior of Fe-based DESs, our group designed a system involving FeCl<sub>3</sub>·6H<sub>2</sub>O/urea DES and Ni foam (NF) with one-step synthesized flower-like NiFe LDH (Figure 7a–e) [130]. Dipping NF into FeCl<sub>3</sub>·6H<sub>2</sub>O/urea would precipitate a series of reactions. A redox reaction between Fe<sup>3+</sup> and NF would make NF become oxidized to Ni<sup>2+</sup>. Then, Fe<sup>3+</sup> and Ni<sup>2+</sup> would

construct NiFe-LDH on the surface of NF, with  $\text{OH}^-$  formed by the hydrolysis of urea. The reaction only took 30 s at 60 °C. Compared with the literature reports [131], reaction conditions in our dipping redox synthetic strategy had clear advantages, such as a mild environment, a simple operation, a low temperature, a rapid reaction, and so on. Moreover, it has been found that urea as HBD could form hydrogen bonds with  $\text{Cl}^-$  while coordinating with  $\text{Fe}^{3+}$  in  $\text{FeCl}_3 \cdot 6\text{H}_2\text{O}/\text{urea}$  DES [125]. These interactions led to distinguishing structural characteristics. The design was more meaningful because urea was adsorbed on the surface of NiFe-LDH, achieving in situ modification of the catalyst resulting from the coordination effect of urea. The combination of urea could improve the flow of electrons and then facilitate the catalysis. Therefore, DES had four functions, medium,  $\text{Fe}^{3+}$  source, oxidant and in situ surface modifier, which realized “four-in-one” synthesis. To further explore the effect of DES on the characteristics of catalysts, we replaced  $\text{FeCl}_3 \cdot 6\text{H}_2\text{O}/\text{urea}$  DES with  $\text{FeCl}_3$  aqueous solution as a control example. In addition to there being no urea modification of NF in an aqueous solution, the etching of NF in aqueous solution was more serious than that in a DES. Moreover, the mass loading of LDH on the NF was lower than that of a DES. In an alkaline medium, the nanoflowered DES-derived catalyst exhibited excellent electrocatalytic activity for OER with a potential of 1.39 V to achieve a current density of  $10 \text{ mA cm}^{-2}$ , which was better than NiFe-LDH/NF obtained from a  $\text{FeCl}_3$  aqueous solution and most of the reported transition-metal catalysts. What is exciting is that the NiFe-LDH obtained from DES could achieve urea oxidation reaction, an anode reaction instead of OER, with the requirement of a potential of 1.32 V. NiFe-LDH/NF as cathode as well as anode could be implemented very well when considering water splitting and urea electrolysis. In this work,  $\text{FeCl}_3 \cdot 6\text{H}_2\text{O}/\text{urea}$  DES was firstly employed to synthesize LDH nanomaterials. From the perspective of environmental protection and reactant utilization, this strategy is a green synthesis method because both HBA and HBD are active components when forming catalysts.  $\text{FeCl}_3$  as HBA is both an oxidant and a metal species. Urea as HBD can not only provide  $\text{OH}^-$  but also realize in situ surface engineering.

Inspired by the above achievements, researchers designed a new type of DES,  $\text{NiCl}_2 \cdot 6\text{H}_2\text{O}/\text{FeCl}_3 \cdot 6\text{H}_2\text{O}/\text{urea}/\text{water}$  [132]. This DES was heated by an ionothermal accompanied thermolysis reaction to obtain NiFe-LDH ultrathin nanosheets hybridized with N-doped carbon quantum dots. Each component in DESs contributed to the structure of a catalyst (Figure 7c-i). Owing to the existence of additional  $\text{H}_2\text{O}$  in the precursor, urea pyrolysis would offer  $\text{NH}_4^+$  and  $\text{OH}^-$ .  $\text{OH}^-$  could react with a metal cation to form hydroxide. Meanwhile, the concentration of  $\text{NH}_3$  or  $\text{NH}_4^+$  formed by urea pyrolysis would be high, which might insert and etch NiFe hydroxide, resulting in forming NiFe-LDH. The addition of water could affect the hydrogen-bonding network between HBAs and HBDs, thereby regulating the supramolecular structure and physicochemical properties of DES [133–135]. The in situ carbonization of the reaction systems led to the generation of N-doped carbon quantum dots, creating the disadvantage that carbon quantum dots need to be prepared in advance. A DES single precursor provided unique surface/interface energy for NiFe-LDH ultrathin nanosheets, making a mesoporous structure with rich defects. Meanwhile, DES ions were more easily inserted into the interlayer, so that the layer could be easily stripped to form ultra-thin nano sheets. Synergy of these factors was beneficial to the improvement of catalytic activity. This catalyst had excellent OER performance ( $\eta_{10} = 252$ ,  $\eta_{100} = 311$ ,  $\eta_{500} = 363 \text{ mV}$  ( $\eta_{100}$  and  $\eta_{500}$  are the overpotentials corresponding to current densities of 100 and 500  $\text{mA cm}^{-2}$ , respectively)). This method provides a feasible and environmentally friendly strategy for the design and synthesis of other carbon hybrid ultra-thin LDH nanosheets with unique electrochemical properties [132].

This method can make both HBAs and HBDs participate in the reactions. To further realize the atomic 100% transformation of reactants, our group developed an “all-in-one” conversion strategy, which was consistent with the concept of green chemistry [136]. We directly heated  $\text{CoCl}_2 \cdot 6\text{H}_2\text{O}/\text{urea}$  DES without adding any other reagents, resulting in the synthesis of 2D nanosheeted  $[\text{Co}(\text{NH}_3)_4\text{CO}_3]\text{Cl}$  via the self-reaction of HBA and HBD,

in which DES had been used simultaneously as a solvent, template, and reactant precursor (Figure 7j–n). We speculated that urea could be hydrolyzed to  $\text{NH}_3$  and  $\text{CO}_2$  under the action of a small amount of water existing in the hydrated metal salt. Then  $\text{NH}_3$  coordinated with  $\text{Co}^{2+}$  to form  $[\text{Co}(\text{NH}_3)_4]^{2+}$ . The oxygen in the reactor could oxidize  $\text{Co}^{2+}$  to  $\text{Co}^{3+}$  under a high temperature and high pressure. Finally,  $[\text{Co}(\text{NH}_3)_4\text{CO}_3]\text{Cl}$  was generated. Nanosheeted  $[\text{Co}(\text{NH}_3)_4\text{CO}_3]\text{Cl}$  could transform into amorphous  $\text{CoOOH}$  during the activation process. It exhibited satisfactory catalytic efficiency ( $\eta_{10} = 291$  mV, Tafel slope =  $65$  mV  $\text{dec}^{-1}$ ) as well as long-term durability (Figure 7o,p). The improved catalytic properties were attributed to rich  $\text{Co}^{3+}$  in  $[\text{Co}(\text{NH}_3)_4\text{CO}_3]\text{Cl}$ . As a catalyst precursor,  $[\text{Co}(\text{NH}_3)_4\text{CO}_3]\text{Cl}$  was converted into  $\text{CoOOH}$  during the activation process, an effective catalytic active component for oxygen evolution. The enriched  $\text{Co}^{3+}$  could not only effectively improve the adsorption energy of the  $\text{H}_2\text{O}$  molecule, but also promote the deprotonation of the  $\text{OOH}^*$  species to form  $\text{O}_2$ . Meanwhile, the 2D activated  $[\text{Co}(\text{NH}_3)_4\text{CO}_3]\text{Cl}$  increased the catalytic area with more exposed electrochemical active sites. The present all-in-one DES strategy opened the door for a reasonable design of DESs and advanced electrocatalysts from a sustainable perspective. By replacing urea in DESs with thiourea,  $\text{CoCl}_2 \cdot 6\text{H}_2\text{O}$ /thiourea DES were obtained [137]. A defect-rich ultrathin N, S, and O tridoped carbon/ $\text{Co}_9\text{S}_8$  was obtained by calcining the carbon cloth coated  $\text{CoCl}_2$ /thiourea evenly. The catalyst had excellent electrocatalytic performance for HER in 1.0 M KOH, 1.0 M PBS, and 0.5 M  $\text{H}_2\text{SO}_4$  electrolytes ( $\eta_{10} = 53, 103$  and 68 mV, respectively).

Fe, Co, and Ni are called the “three musketeers” of electrocatalytic water splitting. To further improve the catalytic performance, it is desirable to combine these elements into one material [138–140]. However, it is difficult to achieve the combination of Fe, Co, and Ni components via conventional methods due to the different reducibility of  $\text{Fe}^{3+}$ ,  $\text{Co}^{2+}$  and  $\text{Ni}^{2+}$ . However, using DESs can easily solve this limitation thanks to the excellent solubility of DESs. Recently, a novel four-component DES, hydrated trimetallic salt/L-cysteine, was designed [141]. HBA included three hydrated metal halides,  $\text{FeCl}_3 \cdot 6\text{H}_2\text{O}$ ,  $\text{CoCl}_2 \cdot 6\text{H}_2\text{O}$  and  $\text{NiCl}_2 \cdot 6\text{H}_2\text{O}$ . L-cysteine containing both  $-\text{COOH}$  and  $-\text{NH}_2$  functional groups acted as HBD. Directly calcinating this DES would produce advanced FeCoNi-based nitro-sulfide (FeCoNi-NS) by the self-reaction of the DES. The DES played multiple roles, including as complexing agent, shape-control agent, solvent, and source of metals N and S. The unique liquid structure of the DES gave the resulting product unique structural advantages, such as uniform dispersion of metal ions, high surface area and porous structure, etc. In addition, Fe, Co, and Ni components coordinated with each other to regulate the electronic structure. Therefore, FeCoNi-NS was conducive to efficient mass/charge transportation. The above characteristics were derived from FeCoNi-NS to improve the catalytic performance. The obtained FeCoNi-NS exhibited excellent OER performance, arriving at a current density of  $10$  mA  $\text{cm}^{-2}$  at an overpotential of 251 mV and low Tafel slope of  $58$  mV  $\text{dec}^{-1}$  in 1.0 M KOH.

Such a simple synthetic strategy is applicable to the manufacture of more multi-metal hierarchical structures for energy storage and conservation. Mu et al. has made new progress in the field of DESs [142]. They designed a novel DES through mixing tetrabutylphosphonium chloride ( $[\text{P}_{4444}]\text{Cl}$ ), ethylene glycol, and five equimolar hydrated metal chlorides ( $\text{FeCl}_3 \cdot 6\text{H}_2\text{O}$ ,  $\text{CoCl}_2 \cdot 6\text{H}_2\text{O}$ ,  $\text{NiCl}_2 \cdot 6\text{H}_2\text{O}$ ,  $\text{MnCl}_2 \cdot 4\text{H}_2\text{O}$  and  $\text{CrCl}_3 \cdot 6\text{H}_2\text{O}$ ). The hydrated metal chlorides and  $[\text{P}_{4444}]\text{Cl}$  acted as HBA, while ethylene glycol served as HBD. This DES was used as a precursor to obtain metal phosphides with high entropy via a one-step in situ phosphorization under an inert atmosphere. The diffraction peaks of X-ray diffraction (XRD) examination as well as energy dispersive X-ray spectroscopy (EDX) elemental mapping revealed that a single crystal structure was produced, although it contained five metal species. This confirmed that the product was a high-entropy metal phosphide (HEMP). This phenomenon was attributed to the homogeneity and processability of DESs. As a bifunctional catalyst, this HEMP presented  $\eta_{10} = 136$  mV for HER as well as  $\eta_{10} = 320$  mV for OER in 1.0 M KOH. It was dramatically

superior to the individual components and  $\text{IrO}_2$  catalyst (440 mV), suggesting its excellent catalytic performance.

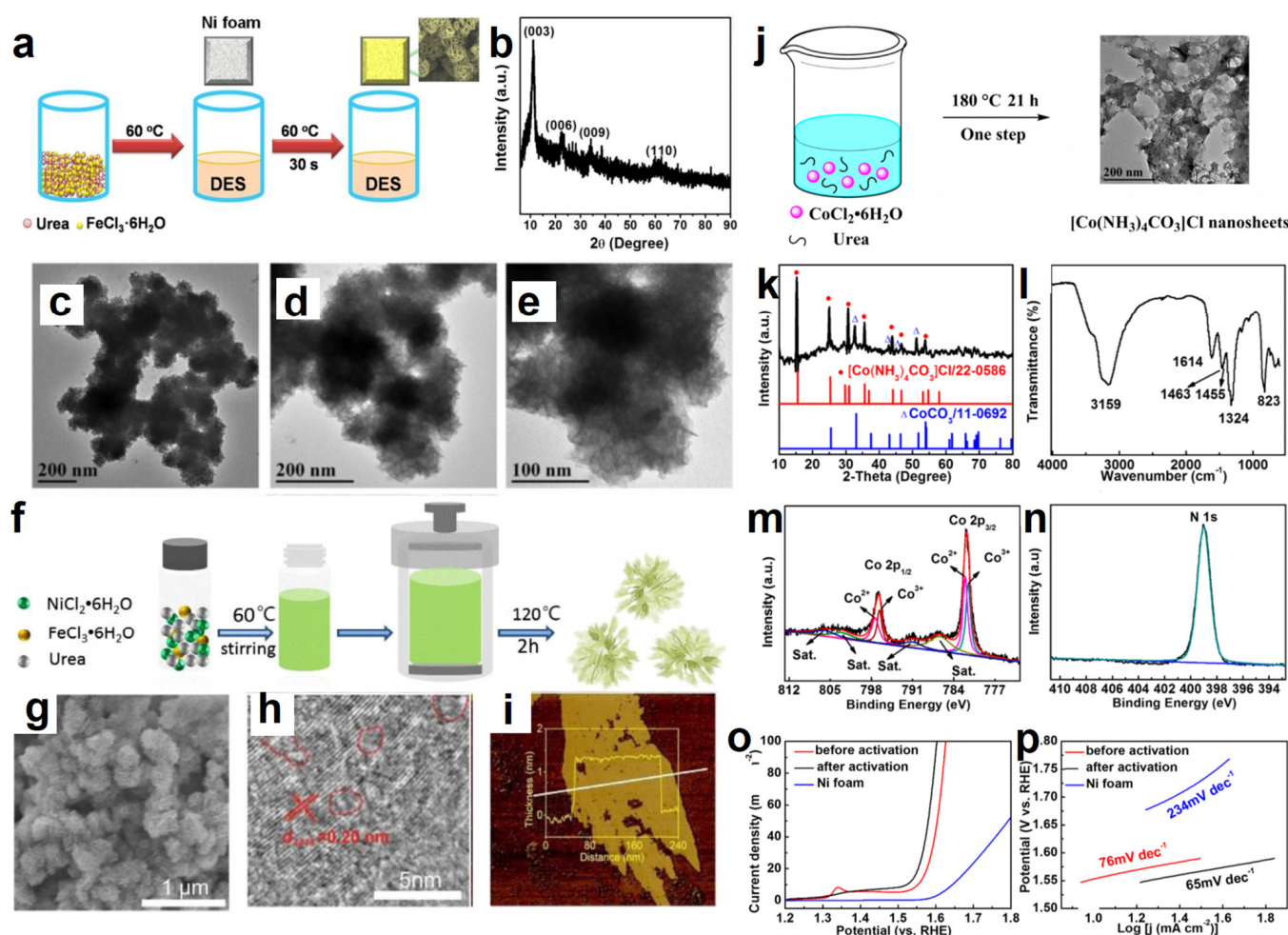


**Figure 7.** Schematic representation of the synthesis of NiFe-LDH/NF (a), XRD of NiFe-LDH (b), SEM images of NiFe-LDH (c–e). Reproduced with permission from ref. [130]. Copyright 2019 Wiley. Synthesis procedure and morphology of the NiFe-LDH/C nanosheets (f), SEM (g), HRTEM (h) and AFM (i) images of NiFe-LDH/C. Reproduced with permission from ref. [132]. Copyright 2021 Elsevier. Typical schematic illustration for synthesis of  $[\text{Co}(\text{NH}_3)_4\text{CO}_3]\text{Cl}$  (j), XRD pattern (k), FT-IR spectra (l) of  $[\text{Co}(\text{NH}_3)_4\text{CO}_3]\text{Cl}$  nanosheets, XPS survey spectrum of Co 2p (m) and N 1s (n) high resolution spectrum, polarization curves (o) and Tafel plots (p) of  $[\text{Co}(\text{NH}_3)_4\text{CO}_3]\text{Cl}$  nanosheets and other catalysts. Reproduced with permission from ref. [136]. Copyright 2019 American Chemical Society.

As can be seen from the above results, the all-in-one DES strategy is an effective measure for preparing metal nanomaterials, and has the following advantages. (1) The supramolecules of DESs can adjust the morphology and catalytic performance of products. (2) The conversion of reactants is close to 100%, reducing emissions and minimizing pollution. (3) The pure DES reactants can lead to the uniform distribution of metal components and good reproducibility. (4) The one-pot process makes the operation simple. DESs as reactive reagents of metal electrocatalysts for HER and OER are summarized in Table 3.

**Table 3.** Summary of HER, OER and Water Splitting Performance of Catalysts Involved in Section 3.

Catalyst	Applied DES	Preparation Method	Catalytic Performance								Ref.
			HER			OER			Water Splitting		
			Electrolyte	$\eta$ (mV)@ Current Density (mA cm <sup>-2</sup> )	Tafel Slope (mV dec <sup>-1</sup> )	Electrolyte	$\eta$ (mV)@ Current Density (mA cm <sup>-2</sup> )	Tafel Slope (mV dec <sup>-1</sup> )	Electrolyte	Potential (V)@ Current Density (mA cm <sup>-2</sup> )	
La <sub>0.5</sub> Sr <sub>0.5</sub> Co <sub>0.8</sub> Fe <sub>0.2</sub> O <sub>3</sub>	Glucose/Urea	Calcining method	—	—	—	1.0 M KOH	304@10	62.9	—	—	[115]
Co@NPC	ChCl/Urea/Gluconic acid ternary	Calcining method	1 M KOH	215@10	70	1 M KOH	430@10	87	1 M KOH	1.74@10	[116]
Iron alkoxide	ChCl/Glycerol	Ionochemical method	—	—	—	1 M KOH	280@10	47	—	—	[117]
NiCo <sub>2</sub> S <sub>4</sub>	PEG 200/Thiourea	Ionochemical method	—	—	—	1 M KOH	337@10	64	—	—	[123]
NiS/Graphene	NiCl <sub>2</sub> ·6H <sub>2</sub> O/PEG 200	Calcining method	1 M KOH	70@10	50.1	1 M KOH	300@10	55.8	1 M KOH	1.54@10	[126]
NiS <sub>2</sub> /Graphene	NiCl <sub>2</sub> ·6H <sub>2</sub> O/Malonic acid	Calcining method	1 M KOH	57@10	47	1 M KOH	294@10	54	1 M KOH	1.52@10	[127]
Ni <sub>2</sub> P/Graphene	NiCl <sub>2</sub> ·6H <sub>2</sub> O/Malonic acid	Calcining method	1 M KOH	103@10	56.5	1 M KOH	275@20	56.2	1 M KOH	1.51@10	[128]
N-C/NiS <sub>2</sub>	NiCl <sub>2</sub> ·6H <sub>2</sub> O/Urea	Calcining method	1 M KOH	78@10	63.4	1 M KOH	264@10	51.3	1 M KOH	1.53@10	[129]
NiFe-LDH	FeCl <sub>3</sub> ·6H <sub>2</sub> O/Urea	Dipping-redox method	1 M KOH	160@10	42	1 M KOH	—	—	1 M KOH	1.61@10	[130]
NiFe-LDH/N-C	NiCl <sub>2</sub> ·6H <sub>2</sub> O/FeCl <sub>3</sub> ·6H <sub>2</sub> O/Urea/Water	Ionochemical method	—	—	—	0.1 M KOH	363@500	49.8	—	—	[132]
[Co(NH <sub>3</sub> ) <sub>4</sub> CO <sub>3</sub> ]Cl	CoCl <sub>2</sub> ·6H <sub>2</sub> O/Urea	Calcining method	—	—	—	1 M KOH	291@10	65	—	—	[136]
N,S,O-C/Co <sub>9</sub> S <sub>8</sub>	CoCl <sub>2</sub> ·6H <sub>2</sub> O/Thiourea	Calcining method	1.0 M KOH	53@10	31	—	—	—	—	—	[137]
N,S,O-C/Co <sub>9</sub> S <sub>8</sub>	CoCl <sub>2</sub> ·6H <sub>2</sub> O/Thiourea	Calcining method	1.0 M PBS	103@10	91.2	—	—	—	—	—	[137]
N,S,O-C/Co <sub>9</sub> S <sub>8</sub>	CoCl <sub>2</sub> ·6H <sub>2</sub> O/Thiourea	Calcining method	0.5 M H <sub>2</sub> SO <sub>4</sub>	68@10	45.3	—	—	—	—	—	[137]
FeCoNi-NS	FeCl <sub>3</sub> ·6H <sub>2</sub> O/CoCl <sub>2</sub> ·6H <sub>2</sub> O/NiCl <sub>2</sub> ·6H <sub>2</sub> O/L-cysteine [P <sub>4444</sub> ]Cl/Ethylene glycol/Five equimolar hydrated metal chlorides	Calcining method	—	—	—	1 M KOH	251@10	58	—	—	[141]
High-entropy metal phosphides	glycol/Five equimolar hydrated metal chlorides	Eutectic solvent method	1 M KOH	136@10	85.5	1 M KOH	320@10	60.8	1 M KOH	1.78@100	[142]

#### 4. Conclusions and Perspectives

DESs have made great developments possible in the area of electrocatalytic water splitting. As solvents and templates, DESs have good solubility, and can dissolve catalyst precursors well. DESs have the capability to regulate growth environment and mechanisms and can control the morphology and size of nanomaterials by their supramolecular structures. As reactants, DESs are safe and efficient when directly participating in the synthesis of catalysts. The designability of DESs allows their composition to be rationally designed to meet the different catalyst components. In the field of synthetic electrocatalysts, DESs have made great achievements. Using DESs can not only synthesize numerous catalysts (metal oxides, sulfides, phosphides, oxide perovskites, etc.), but also control the material structure, simplify the synthesis paths and improve the catalytic performance. The extensive prospects of DESs cause excellent research interest in the field of material synthesis. However, the studies of DES-based electrocatalysts still have some scientific problems to be solved.

##### *4.1. Dialectically Understand the Greenness of DESs and Maximize Their Greenness through Reasonable Design and Effective Control Conditions*

We should dialectically understand the advantages and disadvantages of DESs. At present, DESs are regarded as green solvents to some extent, and have been applied in many fields. However, there is growing evidence that DESs are not always green. Firstly, the hydrogen bond between HBAs and HBDs will be destroyed under certain conditions. We can recognize this point from the fact that DESs can be thermally decomposed to be sources of heteroatoms or metals, as shown in Section 3. In addition, the chemical, electrochemical and radiation decomposition factors can cause the instability of DESs, too. During the decomposition process of DESs, evaporation sometimes occurs, while toxic gases may be generated. This decomposition phenomenon will cause environmental pollution. Meanwhile, the loss of quality also goes against the atomic economy theory. In addition, DESs can react with other substances, which will cause corrosion to other substances. Furthermore, many DESs have been found to be toxic to biological organization in animals, plants, etc., to some extent [143–146]. So DESs are not completely green.

Therefore, it is necessary to explore strategies to improve the green degree of DESs. The designability of DESs, that is, the variable combination of HBDs and HBAs, can give novel DESs with different properties and compositions. Reasonable design composition and control of appropriate conditions will be effective methods to maximize their environmental friendliness [147]. This not only provides more opportunities for the preparation of novel catalysts but also tailors their stability and non-toxicity.

##### *4.2. Requiring Further Understanding of the Structure-Composition-Performance Relationship*

Until now, the role of DESs in the catalyst regulation mechanism and reaction process has been poorly understood. There exists still some randomness in the regulation of catalyst morphology and catalytic performance. It is necessary to further study the participation process of DESs in the nucleation and growth of catalysts, while further analyzing the compositional changes during the reaction process. A particular focus is the fundamental understanding of their structure-composition-performance relationships to realize the rational and controllable design of DES-based catalysts. Meanwhile, scientists should pay special attention to tracking the surface reconstruction process and identifying the real catalytic species under different test conditions, highlighting the significant differences in the corresponding electrochemical reconstruction mechanisms in order to further bridge the gap between laboratory scale research and large-scale application, promoting practical application and accelerating the progress of synergy between material science and engineering [148].

### 4.3. Exploring Research on the Preparation of Single-Atom Catalysts in DESs

Single-atom catalysis has now become one of the new frontiers and hotspots in the field of catalysis. Since single-atom catalysts have the “isolated active sites” characteristics of homogeneous catalysts and the “stable and easy to separate” characteristics of heterogeneous catalysts, they are considered to be expected to open up a new way of heterogenizing homogeneous catalysts and to become a link between homogeneous and heterogeneous catalysts. However, the preparation of single-atom catalysts using DESs has rarely been reported.

**Author Contributions:** C.Z. proposed the topic and drafted the manuscript. Y.F., W.G., T.B., T.C. and J.J. assisted in the literature search and material collection. B.X. checked and revised the manuscript. All authors have read and agreed to the published version of the manuscript.

**Funding:** This work was financially supported by the Natural Science Foundation of the Higher Education Institutions of Jiangsu Province (No. 22KJB150041 and 22KJB150042) Natural Science Foundation of Shandong Province (No. ZR2015EM022 and ZR2022QE227), Shandong Provincial Department of Education 2020 undergraduate teaching reform research project (No. M2020125).

**Institutional Review Board Statement:** Not applicable.

**Informed Consent Statement:** Not applicable.

**Data Availability Statement:** Not applicable.

**Conflicts of Interest:** The authors declare no conflict of interest.

## References

1. Moores, A.; Yan, N. Novel catalytic materials for energy and the environment. *ACS Sustain. Chem. Eng.* **2017**, *5*, 11124. [[CrossRef](#)]
2. Nurul, S.; Kit, W.; Wei, L.; Ratchahat, S.; Rinklebe, J.; Loke, P. Recovery of microalgae biodiesel using liquid biphasic flotation system. *Fuel* **2022**, *317*, 123368.
3. Tang, C.; Zhang, R.; Lu, W.; He, L.; Jiang, X.; Asiri, A.M.; Sun, X. Fe-doped CoP nanoarray: A monolithic multifunctional catalyst for highly efficient hydrogen generation. *Adv. Mater.* **2017**, *29*, 1602441. [[CrossRef](#)] [[PubMed](#)]
4. Dibyendu, G.; Krishnendu, R.; Sarkar, K.; Devi, P.; Kumar, P. Surface plasmon-enhanced carbon dot-embellished multifaceted Si(111) nanoheterostructure for photoelectrochemical water splitting. *ACS Appl. Mater. Interfaces* **2020**, *12*, 28792–28800.
5. Zhang, W.; Lai, W.; Cao, R. Energy-related small molecule activation reactions: Oxygen reduction and hydrogen and oxygen evolution reactions catalyzed by porphyrin- and corrole-based systems. *Chem. Rev.* **2017**, *117*, 3717–3797. [[CrossRef](#)]
6. Ajeet, S.; Jyoti, R.; Samim, H.M.D.; Devaiah, C.; Pravin, P.; Pralay, K.; Dibyajyoti, G.; Sameer, S. MoSe<sub>2</sub>/SnS nanoheterostructures for water splitting. *ACS Appl. Nano Mater.* **2022**, *5*, 4293–4304.
7. Callejas, J.; Read, C.; Roske, C.; Nathan, S.; Raymond, E. Synthesis, characterization, and properties of metal phosphide catalysts for the hydrogen evolution reaction. *Chem. Mater.* **2016**, *28*, 6017–6044. [[CrossRef](#)]
8. Zeng, Y.; Zhao, M.; Huang, Z.; Zhu, W.; Zheng, J.; Jiang, Q.; Wang, Z.; Lang, H. Surface reconstruction of water splitting electrocatalysts. *Adv. Energy Mater.* **2022**, *12*, 2201713. [[CrossRef](#)]
9. Kaur, G.; Kumar, H.; Singla, M. Diverse applications of ionic liquids: A comprehensive review. *J. Mol. Liq.* **2022**, *351*, 118556. [[CrossRef](#)]
10. Monica, D. Ionic liquids: Environment-friendly greener solvents for organic synthesis. *Curr. Org. Synth.* **2022**, *19*, 543–557. [[CrossRef](#)]
11. Gebresilassie, E.G.; Armand, M.; Scrosati, B.; Passerini, S. Energy storage materials synthesized from ionic liquids. *Angew. Chem. Int. Ed.* **2014**, *53*, 13342–13359. [[CrossRef](#)] [[PubMed](#)]
12. Cienfuegos, L.Á.; Robles, R.; Miguel, D.; Cuerva, J.M. Reduction reactions in green solvents: Water, supercritical carbon dioxide, and ionic liquids. *ChemSusChem* **2011**, *4*, 1035–1048. [[CrossRef](#)] [[PubMed](#)]
13. Zhao, D.; Liao, Y.; Zhang, Z. Toxicity of ionic liquids. *Clean: Soil Air Water* **2007**, *35*, 42–48. [[CrossRef](#)]
14. Kudlak, B.; Owczarek, K.; Namieśnik, J. Selected issues related to the toxicity of ionic liquids and deep eutectic solvents—A review. *Environ. Sci. Pollut. Res.* **2015**, *22*, 11975–11992. [[CrossRef](#)]
15. Tao, X.Y.; Li, Q.Z.; Wang, J.; Song, G.L.; Liu, H.M.; Cheng, H.; Yang, Z. Improved whole-cell biocatalysis by addition of deep eutectic solvents and natural deep eutectic solvents. *ACS Sustain. Chem. Eng.* **2017**, *5*, 5713–5722.
16. Shi, R.; Yu, D.; Zhou, F.; Yu, J.; Mu, T. An emerging deep eutectic solvent based on halogen bonds. *Chem. Commun.* **2022**, *58*, 4607–4610. [[CrossRef](#)]
17. Paiva, A.; Matias, A.A.; Duarte, A.R.C. How do we drive deep eutectic systems towards an industrial reality? *Curr. Opin. Green Sustain. Chem.* **2018**, *11*, 81–85. [[CrossRef](#)]

18. Abbott, A.P.; Capper, G.; Davies, D.L.; Raymond, K.R.; Vasuki, T. Novel solvent properties of choline chloride/urea mixtures. *Chem. Commun.* **2003**, *1*, 70–71. [[CrossRef](#)]
19. Cooper, E.R.; Andrews, C.D.; Wheatley, P.S.; Webb, P.B.; Wormald, P.; Morris, R.E. Ionic liquids and eutectic mixtures as solvent and template in the synthesis of zeolite analogues. *Nature* **2004**, *430*, 1012–1016. [[CrossRef](#)]
20. Ge, X.; Gu, C.D.; Wang, X.; Tu, J. Deep eutectic solvents (DESs)-derived advanced functional materials for energy and environmental applications: Challenges, opportunities, and future vision. *J. Mater. Chem. A* **2017**, *5*, 8209–8229. [[CrossRef](#)]
21. Zhang, Q.; Vigier, K.D.O.; Royer, S.; Jérôme, F. Deep eutectic solvents: Synthesis, properties, and applications. *Chem. Soc. Rev.* **2012**, *41*, 7108–7146. [[CrossRef](#)]
22. Catarina, F.; Filipa, L.; Bernardo, D.R.; Martins, M.; Reis, R.L.; Duarte, A.R.C. Natural deep eutectic solvents—Solvents for the 21st century. *ACS Sustain. Chem. Eng.* **2014**, *2*, 1063–1071.
23. Patrycja, J.; Massoud, K.; Justyna, P.; Gębicki, J. Supramolecular deep eutectic solvents and their applications. *Green Chem.* **2022**, *24*, 5035–5045.
24. McDonald, T.R.; Mills, L.R.; West, M.S.; Poe, D.; Zhang, Y.; Klein, J.M.; Horton, A.; Adhikari, L.; Zelovich, T.; Doherty, B.W.; et al. Deep eutectic solvents: A review of fundamentals and applications. *Chem. Rev.* **2021**, *121*, 1232–1285.
25. Abbott, A.P.; Barron, J.C.; Ryder, K.S.; Wilson, D. Eutectic-based ionic liquids with metal-containing anions and cations. *Chem. Eur. J.* **2007**, *13*, 6495–6501. [[CrossRef](#)] [[PubMed](#)]
26. Abranches, D.O.; Martins, M.A.; Silva, L.P.; Schaeffer, N.; Pinho, S.P.; Coutinho, J.A.P. Phenolic hydrogen bond donors in the formation of nonionic deep eutectic solvents: The quest for type V DES. *Chem. Commun.* **2019**, *55*, 10253–10256. [[CrossRef](#)] [[PubMed](#)]
27. Rachiero, G.P.; Berton, P.; Shamshina, J. Deep eutectic solvents: Alternative solvents for biomass-based waste valorization. *Molecules* **2022**, *27*, 6606. [[CrossRef](#)]
28. Abbott, A.P.; Boothby, D.; Capper, G.; Davies, D.L.; Rasheed, R.K. Deep eutectic solvents formed between choline chloride and carboxylic acid: Versatile alternatives to ionic liquids. *J. Am. Chem. Soc.* **2004**, *126*, 9142–9147. [[CrossRef](#)]
29. Yu, D.K.; Xue, Z.M.; Mu, T.C. Eutectics: Formation, properties, and applications. *Chem. Soc. Rev.* **2021**, *50*, 8596–8638. [[CrossRef](#)]
30. Saif, R.; Rafiq, S.; Muhammad, N. Surface tuning of silica by deep eutectic solvent to synthesize biomass derived based membranes for gas separation to enhance the circular bioeconomy. *Fuel* **2022**, *310*, 122355. [[CrossRef](#)]
31. Macfarlane, D.R.; Tachikawa, N.; Forsyth, M.; Pringle, J.M.; Howlett, P.C.; Elliott, G.D.; Davis, J.J.H.; Watanabe, M.; Simon, P.; Angell, A.C. Energy applications of ionic liquids. *Energy Environ. Sci.* **2014**, *7*, 232–250. [[CrossRef](#)]
32. Yu, D.; Xue, Z.; Mu, T. Deep eutectic solvents as a green toolbox for synthesis. *Cell Rep. Phys. Sci.* **2022**, *3*, 100809. [[CrossRef](#)]
33. Hammond, O.S.; Edler, K.J.; Bowron, D.T.; Laura, T.M. Deep eutectic solvothermal synthesis of nanostructured ceria. *Nat. Commun.* **2017**, *8*, 14150. [[CrossRef](#)] [[PubMed](#)]
34. Xu, S.S.; Lv, X.W.; Zhao, Y.M.; Ren, T.Z.; Yuan, Z.Y. Engineering of cobalt oxide/phosphate-carbon nanohybrids for high-efficiency electrochemical water oxidation and reduction. *J. Energy Chem.* **2021**, *52*, 139–146. [[CrossRef](#)]
35. Deng, J.; Fang, S.; Fang, Y.; Hao, Q.; Wang, L.; Hu, Y.H. Multiple roles of graphene in electrocatalysts for metal-air batteries. *Catal. Today* **2022**, *in press*. [[CrossRef](#)]
36. Zhang, C.; Bai, T.; Sun, Y.; Xin, B.; Zhang, S. Ionic Liquid/Deep Eutectic Solvent-Mediated Ni-Based Catalysts and Their Application in Water Splitting Electrocatalysis. *Catalysts* **2022**, *12*, 928. [[CrossRef](#)]
37. Chen, C.H.; Wu, D.; Li, Z.; Zhang, R.; Kuai, C.G.; Zhao, X.R.; Dong, C.K.; Qiao, S.Z.; Liu, H.; Du, X.W. Ruthenium-based single-atom alloy with high electrocatalytic activity for hydrogen evolution. *Adv. Energy Mater.* **2019**, *9*, 1803913. [[CrossRef](#)]
38. Fechler, N.; Zussblatt, N.P.; Rothe, R.; Schlögl, R.; Willinger, M.G.; Chmelka, B.F.; Antonietti, M. Eutectic syntheses of graphitic carbon with high pyrazinic nitrogen content. *Adv. Mater.* **2016**, *28*, 1287–1294. [[CrossRef](#)]
39. Shishov, A.; Chromá, R.; Vakh, C.; Kuchár, J.; Simon, A.; Andruch, V.; Bulatov, A. In situ decomposition of deep eutectic solvent as a novel approach in liquid-liquid microextraction. *Anal. Chim. Acta* **2019**, *1065*, 49–55. [[CrossRef](#)]
40. El Achkar, T.; Greige-Gerges, H.; Fourmentin, S. Basics and properties of deep eutectic solvents: A review. *Environ. Chem. Lett.* **2021**, *19*, 3397–3408. [[CrossRef](#)]
41. Cecilia, O.Z.; Javier, G.S.; Javier, H.B. Deep Eutectic solvents application in food analysis. *Molecules* **2021**, *26*, 6846.
42. Wang, J.; Teng, C.; Yan, L. Applications of deep eutectic solvents in the extraction, dissolution, and functional materials of chitin: Research progress and prospects. *Green Chem.* **2022**, *24*, 552–564. [[CrossRef](#)]
43. Carolin, R.; Burkhard, K. Low melting mixtures in organic synthesis—An alternative to ionic liquids? *Green Chem.* **2012**, *14*, 2969–2982.
44. Durgesh, V.W.; Zhao, H.; Gary, A.B. Deep eutectic solvents: Sustainable media for nanoscale and functional materials. *Acc. Chem. Res.* **2014**, *47*, 2299–2308.
45. Abbott, A.P. Deep eutectic solvents and their application in electrochemistry. *Curr. Opin. Green Sustain. Chem.* **2022**, *36*, 100649. [[CrossRef](#)]
46. Guo, C.; Zhang, B.; Lin, T.; Faaij, A.P.C. Economic optimization for a dual-feedstock lignocellulosic-based sustainable biofuel supply chain considering greenhouse gas emissions and soil carbon stock. *Biofuels Bioprod. Biorefin.* **2022**, *16*, 653–670.
47. Rangaswamy, P.; Chanchal, M.; Dibyendu, M.; Ghosh, D. An account on deep eutectic solvent-based electrolytes for rechargeable batteries and supercapacitors. *Sustain. Mater. Technol.* **2022**, *33*, 477.

48. Kristina, R.; Jelena, Ž.; Marina, C.B. Comparative in vitro study of cholinium-based ionic liquids and deep eutectic solvents on a fish cell line. *Ecotox. Environ. Saf.* **2016**, *131*, 30–36.
49. Cheng, Q.B.; Zhang, L.W. Highly efficient enzymatic preparation of daidzein in deep eutectic solvents. *Molecules* **2017**, *22*, 186. [[CrossRef](#)]
50. Nakhle, L.; Kfoury, M.; Mallard, I.; Landy, D. Microextraction of bioactive compounds using deep eutectic solvents: A review. *Environ. Chem. Lett.* **2021**, *19*, 3747–3759. [[CrossRef](#)]
51. Potka-Wasyłka, J.; Guardia, M.; Andruch, V.; Vilková, M. Deep eutectic solvents vs ionic liquids: Similarities and differences. *Microchem. J.* **2020**, *159*, 105539. [[CrossRef](#)]
52. Abbott, A.P.; Ballantyne, A.; Harris, R.C.; Juma, J.A.; Ryder, K.S.; Forrest, G. A comparative study of nickel electrodeposition using deep eutectic solvents and aqueous solutions. *Electrochim. Acta* **2015**, *176*, 718–726. [[CrossRef](#)]
53. Cruz, H.; Jordão, N.; Branco, L.C. Deep eutectic solvents (DESs) as low-cost and green electrolytes for electrochromic devices. *Green Chem.* **2017**, *19*, 1653. [[CrossRef](#)]
54. Sebastian, P.; Giannotti, M.I.; Gómez, E.; Feliu, J.M. Surface sensitive nickel electrodeposition in deep eutectic solvent. *ACS Appl. Energy Mater.* **2018**, *1*, 1016–1028. [[CrossRef](#)]
55. Elsharkawya, S.; Hammad, S.; El-hallaga, I. Electrodeposition of Ni nanoparticles from deep eutectic solvent and aqueous solution promotes high stability electrocatalyst for hydrogen and oxygen evolution reactions. *J. Solid State Electrochem.* **2022**, *26*, 1501–1517. [[CrossRef](#)]
56. Protsenko, V.S.; Bobrova, L.S.; Korniy, S.A.; Danilov, F.I. Electrochemical synthesis and characterization of electrocatalytic materials for hydrogen production using Cr(III) baths based on a deep eutectic solvent. *Mater. Lett.* **2022**, *313*, 131800. [[CrossRef](#)]
57. Wang, S.; Zou, X.; Lu, Y.; Rao, S.; Xie, X.; Pang, Z.; Lu, X.; Xu, Q.; Zhou, Z. Electrodeposition of nanonickel in deep eutectic solvents for hydrogen evolution reaction in alkaline solution. *Int. J. Hydrogen Energy* **2018**, *43*, 15673–15686. [[CrossRef](#)]
58. Protsenko, V.S.; Bogdanov, D.A.; Korniy, S.A.; Kityk, A.A.; Baskevich, A.S.; Danilov, F.I. Application of a deep eutectic solvent to prepare nanocrystalline Ni and Ni/TiO<sub>2</sub> coatings as electrocatalysts for the hydrogen evolution reaction. *Int. J. Hydrogen Energy* **2019**, *44*, 24604–24616. [[CrossRef](#)]
59. Gao, M.Y.; Sun, C.; Lei, H.; Zeng, J.R.; Zhang, Q.B. Nitrate-induced and in situ electrochemical activation synthesis of oxygen deficiency-rich nickel/nickel (oxy)hydroxide hybrid films for enhanced electrocatalytic water splitting. *Nanoscale* **2018**, *10*, 17546–17551. [[CrossRef](#)]
60. Zeng, J.; Gao, M.Y.; Zhang, Q.; Yang, C.; Li, X.T.; Yang, W.Q.; Hua, Y.X.; Xu, C.Y.; Li, Y. Facile electrodeposition of cauliflower-like S-doped nickel microsphere films as highly active catalysts for electrochemical hydrogen evolution. *J. Mater. Chem. A* **2017**, *5*, 15056–15064. [[CrossRef](#)]
61. Yang, C.; Zhang, Q.; Abbott, A.P. Facile fabrication of nickel nanostructures on a copper-based template via a galvanic replacement reaction in a deep eutectic solvent. *Electrochem. Commun.* **2016**, *70*, 60–64. [[CrossRef](#)]
62. Yang, C.; Gao, M.Y.; Zhang, Q.; Zeng, J.R.; Li, X.T.; Abbott, A.P. In-situ activation of self-supported 3D hierarchically porous Ni<sub>3</sub>S<sub>2</sub> films grown on nanoporous copper as excellent pH-universal electrocatalysts for hydrogen evolution reaction. *Nano Energy* **2017**, *36*, 85–94. [[CrossRef](#)]
63. Zhao, Y.; Zhao, Y.; Feng, H.; Shen, J. Synthesis of nickel phosphide nanoparticles in a eutectic mixture for hydrotreating reactions. *J. Mater. Chem.* **2011**, *21*, 8137–8145. [[CrossRef](#)]
64. Sun, C.; Zeng, J.; Lei, H.; Yang, W.; Zhang, Q. Direct electrodeposition of phosphorus-doped nickel superstructures from choline chloride-ethylene glycol deep eutectic solvent for enhanced hydrogen evolution catalysis. *ACS Sustain. Chem. Eng.* **2019**, *7*, 1529–1537. [[CrossRef](#)]
65. Li, L.; Sheng, S.; Wang, H.; Qu, T.; Hou, D.; Wang, D.; Sheng, M. Electrodeposition of Ni–P alloy in deep eutectic solvent and its electrocatalytic activity toward hydrogen evolution reaction. *Can. J. Chem. Eng.* **2022**, *100*, 3381–3394. [[CrossRef](#)]
66. Gao, M.Y.; Yang, C.; Zhang, Q.; Zeng, J.R.; Li, X.T.; Hua, Y.X.; Xu, C.Y.; Dong, P. Facile electrochemical preparation of self-supported porous Ni–Mo alloy microsphere films as efficient bifunctional electrocatalysts for water splitting. *J. Mater. Chem. A* **2017**, *5*, 5797–5805. [[CrossRef](#)]
67. Lu, Y.; Geng, S.; Wang, S.; Rao, S.; Huang, Y.; Zou, X.; Zhang, Y.; Xu, Q.; Lu, X. Electrodeposition of NiMoCu coatings on roasted nickel matte in deep eutectic solvent for hydrogen evolution reaction. *Int. J. Hydrogen Energy* **2019**, *44*, 5704–5716. [[CrossRef](#)]
68. Gao, M.Y.; Yang, C.; Zhang, Q.; Yu, Y.W.; Hua, Y.X.; Li, Y.; Dong, P. Electrochemical fabrication of porous Ni–Cu alloy nanosheets with high catalytic activity for hydrogen evolution. *Electrochim. Acta* **2016**, *215*, 609–616. [[CrossRef](#)]
69. Vijayakumar, J.; Mohan, S.; Kumar, S.A.; Suseendiran, S.R.; Pavithra, S. Electrodeposition of Ni–Co–Sn alloy in choline chloride-based deep eutectic solvent and characterization as cathode for hydrogen evolution in alkaline solution. *Int. J. Hydrogen Energy* **2013**, *38*, 10208–10214. [[CrossRef](#)]
70. Vo, T.; Hidalgo, S.D.S.; Chiang, C. Controllable electrodeposition of binary metal films from deep eutectic solvent as an efficient and durable catalyst for the oxygen evolution reaction. *Dalton Trans.* **2019**, *48*, 14748–14757. [[CrossRef](#)]
71. Francisco, G.S.; Oliveira, L.P.M.; Santos, R.B.; Silva, R.B.D.; Correa, M.A.; Bohn, F.; Correia, A.N.; Vieira, L.; Vasconcelos, I.F.; Lima-Neto, P. Fe<sub>x</sub>Ni<sub>(1-x)</sub> coatings electrodeposited from choline chloride-urea mixture: Magnetic and electrocatalytic properties for water electrolysis. *Mater. Chem. Phys.* **2022**, *279*, 125738.
72. Sun, C.B.; Guo, M.W.; Siwal, S.S.; Zhang, Q.B. Efficient hydrogen production via urea electrolysis of cobalt-doped nickel hydroxide-riched hybrid films: Cobalt doping effect and mechanism aspects. *J. Catal.* **2020**, *381*, 454–461. [[CrossRef](#)]

73. Zhang, C.; Xin, B.; Chen, T.; Ying, H.; Li, Z.; Hao, J. Deep eutectic solvent strategy enables an octahedral Ni–Co precursor for creating high-performance NiCo<sub>2</sub>O<sub>4</sub> catalyst with oxygen evolution reaction. *Green Energy Environ.* **2022**, *7*, 1217–1227. [[CrossRef](#)]
74. Yang, H.Y.; Cheng, Z.F.; Wu, P.C.; Wei, Y.; Jiang, J.; Xu, Q. Deep eutectic solvent regulation synthesis of multimetal oxalate for electrocatalytic oxygen evolution reaction and supercapacitor applications. *Electrochim. Acta* **2022**, *427*, 140879. [[CrossRef](#)]
75. Zhang, Y.; Ru, J.; Hua, Y.; Huang, P.; Xu, C. One-step preparation, and adsorption property of mesoporous nickel sulfides in deep eutectic solvent. *Ceram. Int.* **2022**, *48*, 20341–20350. [[CrossRef](#)]
76. Gao, M.; Zeng, J.; Zhang, Q.; Yang, C.; Li, X.T.; Hua, Y.X.; Xu, C.Y. Scalable one-step electrochemical deposition of nanoporous amorphous S-doped NiFe<sub>2</sub>O<sub>4</sub>/Ni<sub>3</sub>Fe composite films as highly efficient electrocatalysts for oxygen evolution with ultrahigh stability. *J. Mater. Chem. A* **2018**, *6*, 1551–1560. [[CrossRef](#)]
77. Zeng, J.; Liu, J.; Siwal, S.S.; Yang, W.; Fu, X.; Zhang, Q. Morphological and electronic modification of 3D porous nickel microsphere arrays by cobalt and sulfur dual synergistic modulation for overall water splitting electrolysis and supercapacitors. *Appl. Surf. Sci.* **2019**, *491*, 570–578. [[CrossRef](#)]
78. Renjith, A.; Lakshminarayanan, V. Single-step electrochemical synthesis of cobalt nanoclusters embedded in dense graphite sheets for electrocatalysis of the oxygen evolution reaction. *ACS Appl. Nano Mater.* **2020**, *3*, 2705–2712. [[CrossRef](#)]
79. Li, K.; Ren, T.; Yuan, Z.; Badosz, T.J. Electrodeposited P–Co nanoparticles in deep eutectic solvents and their performance in water splitting. *Int. J. Hydrogen Energy* **2018**, *43*, 10448–10457. [[CrossRef](#)]
80. Yang, W.; Hua, Y.X.; Zhang, Q.; Lei, H.; Xu, C.Y. Electrochemical fabrication of 3D quasi-amorphous pompon-ike Co–O and Co–Se hybrid films from choline chloride/urea deep eutectic solvent for efficient overall water splitting. *Electrochim. Acta* **2018**, *273*, 71–79. [[CrossRef](#)]
81. Yang, W.; Zeng, J.; Hua, Y.; Xu, C.; Siwal, S.S.; Zhang, Q. Defect engineering of cobalt microspheres by S doping and electrochemical oxidation as efficient, bifunctional, and durable electrocatalysts for water splitting at high current densities. *J. Power Sources* **2019**, *436*, 226887. [[CrossRef](#)]
82. Zhao, X.; Jiang, J.; Xue, Z.; Yan, C.; Mu, T. An ambient temperature, CO<sub>2</sub>-assisted solution processing of amorphous cobalt sulfide in a thiol/amine based quasi-ionic liquid for oxygen evolution catalysis. *Chem. Commun.* **2017**, *53*, 9418–9421. [[CrossRef](#)] [[PubMed](#)]
83. Thorat, G.M.; Jadhav, H.S.; Roy, A.; Chung, W.; Seo, J.G. Dual role of deep eutectic solvent as a solvent and template for the synthesis of octahedral cobalt vanadate by an oxygen evolution reaction. *ACS Sustain. Chem. Eng.* **2018**, *6*, 16255–16266. [[CrossRef](#)]
84. Liu, J.; Ji, Y.; Nai, J.; Niu, X.; Luo, Y.; Guo, L.; Yang, S. Ultrathin amorphous cobalt-vanadium hydr(oxy)oxide catalysts for the oxygen evolution reaction. *Energy Environ. Sci.* **2018**, *11*, 1736–1741. [[CrossRef](#)]
85. Liardet, L.; Hu, X. Amorphous Cobalt vanadium oxide as a highly active electrocatalyst for oxygen evolution. *ACS Catal.* **2018**, *8*, 644–650. [[CrossRef](#)] [[PubMed](#)]
86. Corrigan, D.A. The catalysis of the oxygen evolution reaction by iron impurities in thin film nickel oxide electrodes. *J. Electrochem. Soc.* **1987**, *134*, 377–384. [[CrossRef](#)]
87. Burke, M.S.; Kast, M.G.; Trotochaud, L.; Smith, A.M.; Boettcher, S.W. Cobalt-iron (oxy)hydroxide oxygen evolution electrocatalysts: The role of structure and composition on activity, stability, and mechanism. *J. Am. Chem. Soc.* **2015**, *137*, 3638–3648. [[CrossRef](#)]
88. Ge, X.; Gu, C.D.; Wang, X.L.; Tu, J.P. Ionothermal synthesis of cobalt iron layered double hydroxides (LDHs) with expanded interlayer spacing as advanced electrochemical materials. *J. Mater. Chem. A* **2014**, *2*, 17066–17076. [[CrossRef](#)]
89. Ge, X.; Gu, C.D.; Lu, Y.; Wang, X.L.; Tu, J.P. A versatile protocol for the ionothermal synthesis of nanostructured nickel compounds as energy storage materials from a choline chloride-based ionic liquid. *J. Mater. Chem. A* **2013**, *1*, 13454–13461. [[CrossRef](#)]
90. Ge, X.; Gu, C.D.; Wang, X.L.; Tu, J.P. Correlation between microstructure and electrochemical behavior of the mesoporous Co<sub>3</sub>O<sub>4</sub> sheet and its ionothermal synthesized hydrotalcite-like α-Co(OH)<sub>2</sub> precursor. *J. Phys. Chem. C* **2014**, *118*, 911–923. [[CrossRef](#)]
91. Yang, C.; He, T.; Zhou, W.; Deng, R.; Zhang, Q. Iron-tuned 3D cobalt-phosphate catalysts for efficient hydrogen and oxygen evolution reactions over a wide pH range. *ACS Sustain. Chem. Eng.* **2020**, *8*, 13793–13804. [[CrossRef](#)]
92. Wang, W.; Xu, R.; Yu, B.; Wang, X.; Feng, S. Electrochemical fabrication of FeS<sub>x</sub> films with high catalytic activity for oxygen evolution. *RSC Adv.* **2019**, *9*, 31979–31987. [[CrossRef](#)] [[PubMed](#)]
93. Liu, S.; Chen, T.; Ying, H.; Hao, J. Deep eutectic solvent-mediated construction of oxygen vacancy-rich Fe-based electrocatalysts for efficient oxygen evolution reaction. *Adv. Sustain. Syst.* **2020**, *4*, 2000038. [[CrossRef](#)]
94. Guo, M.; Wei, Z.; Zhang, Q. Electrochemical construction of S-doped MnO/Mn integrated film on carbon paper in a choline deep eutectic solvent for enhanced electrochemical water oxidation. *Int. J. Hydrogen Energy* **2022**, *47*, 6029–6043. [[CrossRef](#)]
95. Hong, S.; Díez, A.M.; Adedoyin, N.A.; Sousa, J.P.S.; Salonen, L.M.; Lebedev, O.I.; Kolen'ko, Y.V.; Zaikina, J.V. Deep eutectic solvent synthesis of perovskite electrocatalysts for water oxidation. *ACS Appl. Mater. Interfaces* **2022**, *14*, 23277–23284. [[CrossRef](#)]
96. Kumar-Krishnan, S.; Prokhorov, E.; Arias de Fuentes, O.; Ramírez, M.; Bogdanchikova, N.; Sanchez, I.C.; Mota-Morales, J.D.; Luna-Bárcenas, G. Temperature-induced Au nanostructure synthesis in a nonaqueous deep-eutectic solvent for high performance electrocatalysis. *J. Mater. Chem. A* **2015**, *3*, 15869–15875. [[CrossRef](#)]
97. Yang, C.; Lei, H.; Zhou, W.Z.; Zeng, J.R.; Zhang, Q.B.; Hua, Y.X.; Xu, C.Y. Engineering nanoporous Ag/Pd core/shell interfaces with ultrathin Pt doping for efficient hydrogen evolution reaction over a wide pH range. *J. Mater. Chem. A* **2018**, *6*, 14281–14290. [[CrossRef](#)]
98. Smith, E.L.; Abbott, A.P.; Ryder, K.S. Deep eutectic solvents (DESs) and their applications. *Chem. Rev.* **2014**, *114*, 11060–11082. [[CrossRef](#)] [[PubMed](#)]

99. Edison, T.N.J.I.; Atchudan, R.; Karthik, N.; Chandrasekaran, S.; Perumal, S.; Raja, P.B.; Perumal, V.; Lee, Y.R. Deep eutectic solvent assisted electrosynthesis of ruthenium nanoparticles on stainless steel mesh for electrocatalytic hydrogen evolution reaction. *Fuel* **2021**, *297*, 120786. [[CrossRef](#)]
100. Cao, Y.; Guo, S.; Yu, C.; Zhang, J.; Pan, X.; Li, G. Ionic liquid-assisted one-step preparation of ultrafine amorphous metallic hydroxide nanoparticles for the highly efficient oxygen evolution reaction. *J. Mater. Chem. A* **2020**, *8*, 15767–15773. [[CrossRef](#)]
101. Chen, Y.; Li, C.; Chen, P. Galvanic displacement of electrodeposited tangled Zn nanowire sacrificial template for preparing porous and hollow Ni electrodes in ionic liquid. *J. Mol. Liq.* **2020**, *298*, 112050. [[CrossRef](#)]
102. Abdelkader, A.M.; Patten, H.V.; Li, Z.; Chen, Y.; Kinloch, I.A. Electrochemical exfoliation of graphite in quaternary ammonium-based deep eutectic solvents: A route for the mass production of graphane. *Nanoscale* **2015**, *7*, 11386–11392. [[CrossRef](#)] [[PubMed](#)]
103. Zhang, Y.; Xu, Y.; Zhu, J.; Li, L.; Du, X.; Sun, X. Electrochemically exfoliated high-yield graphene in ambient temperature molten salts and its application for flexible solid-state supercapacitors. *Carbon* **2018**, *127*, 392–403. [[CrossRef](#)]
104. Abdelkader, A.M.; Kinloch, I.A. Mechanochemical exfoliation of 2D crystals in deep eutectic solvents. *ACS Sustain. Chem. Eng.* **2016**, *4*, 4465. [[CrossRef](#)]
105. Mohammadpour, Z.; Abdollahi, S.H.; Safavi, A. Sugar-based natural deep eutectic mixtures as green intercalating solvents for high-yield preparation of stable MoS<sub>2</sub> nanosheets: Application to electrocatalysis of hydrogen evolution reaction. *ACS Appl. Energy Mater.* **2018**, *1*, 5896–5906. [[CrossRef](#)]
106. Mohammadpour, Z.; Abdollahi, S.H.; Omidvar, A.; Mohajeri, A.; Safavi, A. Aqueous solutions of carbohydrates are new choices of green solvents for highly efficient exfoliation of two-dimensional nanomaterials. *J. Mol. Liq.* **2020**, *309*, 113087. [[CrossRef](#)]
107. Zhang, T.; Doert, T.; Wang, H.; Zhang, S.; Ruck, M. Inorganic synthesis based on reactions of ionic liquids and deep eutectic solvents. *Angew. Chem. Int. Ed.* **2021**, *60*, 22148–22165. [[CrossRef](#)]
108. Pariiska, O.; Mazur, D.; Cherchenko, K.; Zhang, S.; Ruck, M. Efficient Co–NC electrocatalysts for oxygen reduction derived from deep eutectic solvents. *Electrochim. Acta* **2022**, *413*, 140132. [[CrossRef](#)]
109. Titirici, M.M.; White, R.J.; Brun, N.; Budarin, V.L.; Sheng, S.D.; Monte, F.; Clark, J.H.; MacLachlan, M.J. Sustainable carbon materials. *Chem. Soc. Rev.* **2015**, *44*, 250–290. [[CrossRef](#)]
110. Brandão, A.T.; Costa, R.; Silva, A.F.; Pereira, C.M. Sustainable preparation of nanoporous carbons via dry ball milling: Electrochemical studies using nanocarbon composite electrodes and a deep eutectic solvent as electrolyte. *Nanomaterials* **2021**, *11*, 3258. [[CrossRef](#)]
111. Zhang, J.J.; Sun, Y.; Guo, L.K. Using urea to improve the ORR performance of N-, P-, and S-ternary-doped porous carbon derived from biomass. *Mod. Phys. Lett. B* **2022**, *36*, 2242018. [[CrossRef](#)]
112. Zhu, C.; Li, H.; Fu, S.; Du, D.; Lin, Y. Highly efficient nonprecious metal catalysts towards oxygen reduction reaction based on three-dimensional porous carbon nanostructures. *Chem. Soc. Rev.* **2016**, *45*, 517–531. [[CrossRef](#)] [[PubMed](#)]
113. Deng, W.; Zhang, Q.; Wang, Y. Catalytic transformation of cellulose and cellulose-derived carbohydrates into organic acids. *Catal. Today* **2014**, *234*, 31–41. [[CrossRef](#)]
114. Gutiérrez, M.C.; Rubio, F.; Monte, F.D. Resorcinol-formaldehyde polycondensation in deep eutectic solvents for the preparation of carbons and carbon–carbon nanotube composites. *Chem. Mater.* **2010**, *22*, 2711. [[CrossRef](#)]
115. Rong, K.; Wei, J.; Huang, L.; Fang, Y.; Dong, S. Synthesis of low-dimensional hierarchical transition metal oxides via a direct deep eutectic solvent calcining method for enhanced oxygen evolution catalysis. *Nanoscale* **2020**, *12*, 20719–20725. [[CrossRef](#)]
116. Li, D.; Huang, Y.; Li, Z.; Zhong, L.; Liu, C.; Peng, X. Deep eutectic solvent derived carbon-based efficient electrocatalyst for boosting H<sub>2</sub> production coupled with glucose oxidation. *Chem. Eng. J.* **2022**, *430*, 132783. [[CrossRef](#)]
117. Zhang, C.; Zhang, B.; Li, Z.; Hao, J. Deep eutectic solvent-mediated hierarchically structured Fe-based organic-inorganic hybrid catalyst for oxygen evolution reaction. *ACS Appl. Energy Mater.* **2019**, *2*, 3343–3351. [[CrossRef](#)]
118. Song, S.; Zhou, J.; Su, X.; Wang, Y.; Li, J.; Zhang, L.; Xiao, G.; Guan, C.; Liu, R.; Chen, S.; et al. Operando X-ray spectroscopic tracking of self-reconstruction for anchored nanoparticles as high-performance electrocatalysts towards oxygen evolution. *Energy Environ. Sci.* **2018**, *11*, 2945–2953. [[CrossRef](#)]
119. Shi, Y.; Yu, Y.; Liang, Y.; Du, Y.; Zhang, B. In situ electrochemical conversion of an ultrathin tannin-nickel-iron complex film as an efficient oxygen evolution reaction electrocatalyst. *Angew. Chem.* **2019**, *58*, 3769–3773. [[CrossRef](#)]
120. Niu, S.; Jiang, W.; Wei, Z.; Tang, T.; Ma, J.; Hu, J.S.; Wan, L.J. Se-doping activates FeOOH for cost-effective and efficient electrochemical water oxidation. *J. Am. Chem. Soc.* **2019**, *141*, 7005–7013. [[CrossRef](#)]
121. Chen, H.; Jiang, J.; Zhang, L. Highly conductive NiCo<sub>2</sub>S<sub>4</sub> urchin-like nanostructures for high-rate pseudocapacitors. *Nanoscale* **2013**, *5*, 8879–8883. [[CrossRef](#)] [[PubMed](#)]
122. Lu, F.; Zhou, M.; Li, W.; Li, C.; Xue, Y.; Jiang, X.; Zeng, X.; Bando, Y.; Golberg, D. Engineering sulfur vacancies and impurities in NiCo<sub>2</sub>S<sub>4</sub> nanostructures with optimal supercapacitive performance. *Nano Energy* **2016**, *26*, 313–323. [[CrossRef](#)]
123. Jiang, J.; Yan, C.; Zhao, X.; Luo, H.; Xue, Z.; Mu, T. A PEGylated deep eutectic solvent for controllable solvothermal synthesis of porous NiCo<sub>2</sub>S<sub>4</sub> for efficient oxygen evolution reaction. *Green Chem.* **2017**, *19*, 3023–3031. [[CrossRef](#)]
124. Zhao, X.; Lan, X.; Yu, D.; Fu, H.; Liu, Z.; Mu, T. Deep eutectic solvothermal synthesis of nanostructured Fe<sub>3</sub>S<sub>4</sub> by electrochemical N<sub>2</sub> fixation under ambient conditions. *Chem. Commun.* **2018**, *54*, 13010–13013. [[CrossRef](#)] [[PubMed](#)]
125. Wang, Y.; Zhou, H. A green and cost-effective rechargeable battery with high energy density based on a deep eutectic catholyte. *Energy Environ. Sci.* **2016**, *9*, 2267–2272. [[CrossRef](#)]

126. Zhang, D.; Mou, H.; Lu, F.; Song, C.; Wang, D. A novel strategy for 2D/2D NiS/graphene heterostructures as efficient bifunctional electrocatalysts for overall water splitting. *Appl. Catal. B* **2019**, *254*, 471–478. [[CrossRef](#)]
127. Zhang, D.; Mou, H.; Chen, L.; Wang, D.; Song, C. Design and in-situ synthesis of a unique catalyst via embedding graphene oxide shell membrane in NiS<sub>2</sub> for efficient hydrogen evolution. *Appl. Surf. Sci.* **2020**, *510*, 145483. [[CrossRef](#)]
128. Mou, H.; Wang, J.F.; Yu, D.; Zhang, D.; Lu, F.; Chen, L.; Wang, D.; Mu, T. A facile and controllable, deep eutectic solvent aided strategy for synthesis graphene encapsulated metal phosphides for enhanced electrocatalytic overall water splitting. *J. Mater. Chem. A* **2019**, *7*, 13455–13459. [[CrossRef](#)]
129. Zhang, D.; Mou, H.; Chen, L.; Xing, G.; Wang, D.; Song, C. Surface/interface engineering N-doped carbon/NiS<sub>2</sub> nanosheets for efficient electrocatalytic H<sub>2</sub>O splitting. *Nanoscale* **2020**, *12*, 3370–3376. [[CrossRef](#)]
130. Zhang, C.; Chen, T.; Zhang, H.; Li, Z.; Hao, J. Hydrated metal halide-based deep eutectic solvent-mediated NiFe layered double hydroxide: An excellent electrocatalyst for urea electrolysis and water splitting. *Chem. Asian J.* **2019**, *14*, 2995–3002. [[CrossRef](#)]
131. Gao, Z.; Xie, S.; Zhang, B.; Qiu, X.; Chen, F. Ultrathin Mg–Al layered double hydroxide prepared by ionothermal synthesis in a deep eutectic solvent for highly effective boron removal. *Chem. Eng. J.* **2017**, *319*, 108–118. [[CrossRef](#)]
132. Hu, Z.; Zhang, D.; Sun, C.; Song, C.; Wang, D. One-step ionothermal accompanied thermolysis strategy for N-doped carbon quantum dot hybridized NiFe LDH ultrathin nanosheets for electrocatalytic water oxidation. *Electrochim. Acta* **2021**, *391*, 138932. [[CrossRef](#)]
133. Chen, Y.; Yu, D.; Chen, W.; Li, F.; Mu, T. Water absorption by deep eutectic solvents. *Phys. Chem. Chem. Phys.* **2019**, *21*, 2601–2610. [[CrossRef](#)]
134. Kivelä, H.; Salomäki, M.; Vainikka, P.; Mäkilä, E.; Poletti, F.; Ruggeri, S.; Terzi, F.; Lukkari, J. Effect of water on a hydrophobic deep eutectic solvent. *J. Phys. Chem. B* **2022**, *126*, 513–527. [[CrossRef](#)]
135. Tracy, E.A.; Sophie, F.; Hélène, G.G. Deep eutectic solvents: An overview on their interactions with water and biochemical compounds. *J. Mol. Liq.* **2019**, *288*, 111028.
136. Liu, S.; Zhang, C.; Zhang, B.; Li, Z.; Hao, J. All-in-one deep eutectic solvent with cobalt-based electrocatalyst for oxygen evolution reaction. *ACS Sustain. Chem. Eng.* **2019**, *7*, 8964–8971. [[CrossRef](#)]
137. Mou, H.; Xue, Z.; Zhang, B.; Xue, L.; Mu, T. A deep eutectic solvent strategy to form defect-rich N, S, and O tridoped carbon/Co<sub>9</sub>S<sub>8</sub> hybrid materials by a pH-universal hydrogen evolution reaction. *J. Mater. Chem. A* **2021**, *9*, 2099–2103. [[CrossRef](#)]
138. Li, X.; Duan, F.; Deng, M.; Zheng, W.; Lin, Y.; Dan, Y.; Cheng, X.; Chen, L. Effect of Fe doping on Co–S/carbon cloth as bifunctional electrocatalyst for enhanced water splitting. *J. Electroanal. Chem.* **2022**, *922*, 116723. [[CrossRef](#)]
139. Sun, L.; Wang, C.; Sun, Q.; Cheng, Y.; Wang, L. Self-assembly of hierarchical Ni–Mo–polydopamine microflowers and their conversion to a Ni–Mo<sub>2</sub>C/C composite for water splitting. *Chem. Eur. J.* **2017**, *23*, 4644–4650. [[CrossRef](#)]
140. Rimpa, K.; Madhupriya, S.; Shrabani, G.; Sankar, D.N.; Chattopadhyay, K.K. Co incorporated Ni<sub>3</sub>S<sub>2</sub> hierarchical nano/micro cactus for electrochemical water splitting. *Int. J. Hydrogen Energy* **2019**, *44*, 21315–21323.
141. Jiang, J.; Chang, L.; Zhao, W.; Tian, Q.; Xu, Q. An advanced FeCoNi nitro-sulfide hierarchical structure in deep eutectic solvents for enhanced oxygen evolution reaction. *Chem. Commun.* **2019**, *55*, 10174–10177. [[CrossRef](#)]
142. Zhao, X.; Xue, Z.; Chen, W.; Wang, Y.; Mu, T. Eutectic synthesis of high-entropy metal phosphides for electrocatalytic water splitting. *ChemSusChem* **2020**, *13*, 2038–2042. [[CrossRef](#)]
143. Samori, C.; Mazzei, L.; Ciurli, S.; Cravotto, G.; Grillo, G.; Guidi, E.; Pasteris, A.; Tabasso, S.; Galletti, P. Urease inhibitory potential and soil ecotoxicity of novel “polyphenols-deep eutectic solvents” formulations. *ACS Sustain. Chem. Eng.* **2019**, *7*, 15558–15567. [[CrossRef](#)]
144. de Morais, P.; Goncalves, F.; Coutinho, J.A.P.; Ventura, S.P.M. Ecotoxicity of cholinium-based deep eutectic solvents. *ACS Sustain. Chem. Eng.* **2015**, *3*, 3398–3404. [[CrossRef](#)]
145. Ahmadi, R.; Hemmateenejad, B.; Safavi, A.; Shojaeifard, Z.; Mohabbati, M.; Firuzi, O. Assessment of cytotoxicity of choline chloride-based natural deep eutectic solvents against human HEK–293 cells: A QSAR analysis. *Chemosphere* **2018**, *209*, 831–838. [[CrossRef](#)]
146. Macario, I.P.E.; Oliveira, H.; Menezes, A.C.; Ventura, S.P.M.; Pereira, J.L.; Goncalves, A.M.M.; Coutinho, J.A.P.; Goncalves, F.J.M. Cytotoxicity profiling of deep eutectic solvents to human skin cells. *Sci. Rep.* **2019**, *9*, 3932. [[CrossRef](#)]
147. Chen, Y.; Mu, T.C. Revisiting greenness of ionic liquids and deep eutectic solvents. *Green Chem. Eng.* **2021**, *2*, 174–186. [[CrossRef](#)]
148. Sun, H.; Xu, X.; Kim, H.; Jung, W.; Zhou, W.; Shao, Z. Electrochemical water splitting: Bridging the gaps between fundamental research and industrial applications. *Energy Environ. Mater* **2022**, e12441. [[CrossRef](#)]